5-2023

Force Coefficients and Wind Loads for Wide Flange Section and Retrofitted Pipe Racks

Sovanroth Ou
Clemson University, sovanro@clemson.edu

Force Coefficients and Wind Loads for Wide Flange Section and Retrofitted Pipe Racks

---

A Thesis
Presented to
the Graduate School of
Clemson University

In Partial Fulfillment
of the Requirements for the Degree
Master of Civil Engineering
Civil Engineering

---

by
Sovanroth Ou
May 2023

Accepted by:
Dr. Weichiang Pang, Committee Chair
Dr. Michael Stoner, Committee Co-Chair
Dr. Nigel Kaye

Abstract

Taken from: *Drag Coefficients and Wind Loads of Retrofitted Pipe Racks with High Blockage Ratio* [13].

While relatively rare, the failures of steel structures occasionally occur due to extreme wind events such as hurricanes and tornadoes. The American Society of Civil Engineers (ASCE) provides well-defined guidelines for determining wind loads for regular buildings; nonetheless, the actual wind loads for complex open-frame steel structures are not as clearly understood by practicing engineers. Pipe bridges and pipe racks are open-frame structures, commonly used in many petrochemical plants. Over the years, additional pipes are often added to existing pipe racks or pipe bridges to accommodate changes in the operation needs of the petrochemical plant. The objectives of this study are to investigate (1) the wind loads on wide flange sections using the wind tunnel procedure, (2) strategies to retrofit the pipe racks to accommodate additional pipes, and (3) load distribution during an event where a column loses its load-carrying capacity.

Dedication

This work is dedicated to my supportive family and relatives, especially my mom Samphas Pith.

Acknowledgments

Foremost, I would like to express my sincere gratitude to my advisors, Dr. Weichiang Pang and Dr. Michael Stoner, for the continuous support of my study and research, for their patience, motivation, and immense knowledge.

Besides my advisors, I would like to thank my committee member, Dr. Nigel Kaye, for providing the necessary space and equipment for wind tunnel tests.

My sincere appreciation goes to my fellow friends, Bibek Bhardwaj, Lancelot Reres, Harsh Bothra, and Jayson Leonard, for the excellent discussions and support. I am thankful for the help, advice, and suggestions throughout this study.

Last but not least, I would like to extend my appreciation to my mom, Samphas Pith, for giving birth to me and supporting me throughout my life. I am grateful to my uncle Prakath Pith, my grandma Keav Ith, my brother Sovanrith Ou, and my sister Sovitheavy Ou, for their support along this journey.

I am grateful that Clemson Civil Engineering Department and Virginia Carolinas Structural Fabricators Association (VCSSFA) support the experiments and analyses presented herein. Any opinions, findings, and conclusions presented in this study are those of the authors and do not necessarily reflect the Clemson Civil Engineering Department and VCSSFA's views.

Table of Contents

List of Tables

List of Figures

Chapter 1

Introduction

Partially taken from: *Drag Coefficients and Wind Loads of Retrofitted Pipe Racks with High Blockage Ratio* [13].

Once adequately designed and constructed, the steel frame is one of the most reliable and resilient structural systems. There are many applications for steel frame structures; one of which is as pipe racks in petrochemical plants. In industrial plants, there are occasionally necessities for expansion, resulting in additional mass on the pipe racks. Instead of constructing new ones, retrofitting existing pipe racks to accommodate more pipes is often done. The American Society of Civil Engineers document 7 (ASCE 7), Minimum Design Loads and Associated Criteria for Buildings and Other Structures, has well-defined guidelines for determining wind loads for regular buildings [3]. However, the actual wind load and drag coefficients for open-frame steel structures such as pipe racks are relatively less well understood. In 1989, The Australia Standards (AS 1170) provided sets of drag coefficients for wide flange cross-sections [6], and in 2011, the ASCE Task Committee on Wind-Induced Forces published guidelines for determining drag coefficients for open-frame structures [15].

While the guidelines for designing new pipe racks and pipe bridges are available, there is a scant body of knowledge on how to consider wind loads on a retrofitted open-frame steel structure. This thesis presents the force coefficients for the wide flange section and retrofitted pipe racks determined experimentally via a series of force balance tests using a wind tunnel. The overarching goal of this research is (1) to quantify the force coefficients of wide flange sections, (2) to study the responses of wind loads for retrofitted pipe racks, and (3) to evaluate changes in load distribution in a pipe rack due to missing load path (e.g. a column losing its load-carrying capacity due to

corrosion).

1.1 Historical Performance

Numerious industrial facilities located on the Atlantic coastlines and Gulf have encountered either tropical storms or minor hurricanes and appeared to have functioned effectively [15]. As a result, some people in the industry have developed a misunderstanding that their facilities can endure major hurricane-force winds without suffering significant damage. This belief is based on the fact that many of these facilities have not encountered a design-level event, which is typically a moderate Category 2 or stronger hurricane. There have been several papers published in an attempt to address this issue. Godoy points out the inconsistency of the performance of oil storage tanks [9]. On the other hand, Calvert and Fouad discussed the poor performance of electrical power transmission [5]. Similarly, open-frame structures such as pipe racks can be vulnerable during extreme wind conditions.

During Hurricane Katrina (2005) and Rita (2005), there was severe damage across industrial facilities. The power supply was greatly impacted, with wind forces causing the collapse of roughly a million wooden poles and 300 towers/steel poles. Several steel structures were also severely damaged, including pipe racks and pipe bridges. Figure 1.1 shows a damaged pipe rack during Hurricane Rita.

,

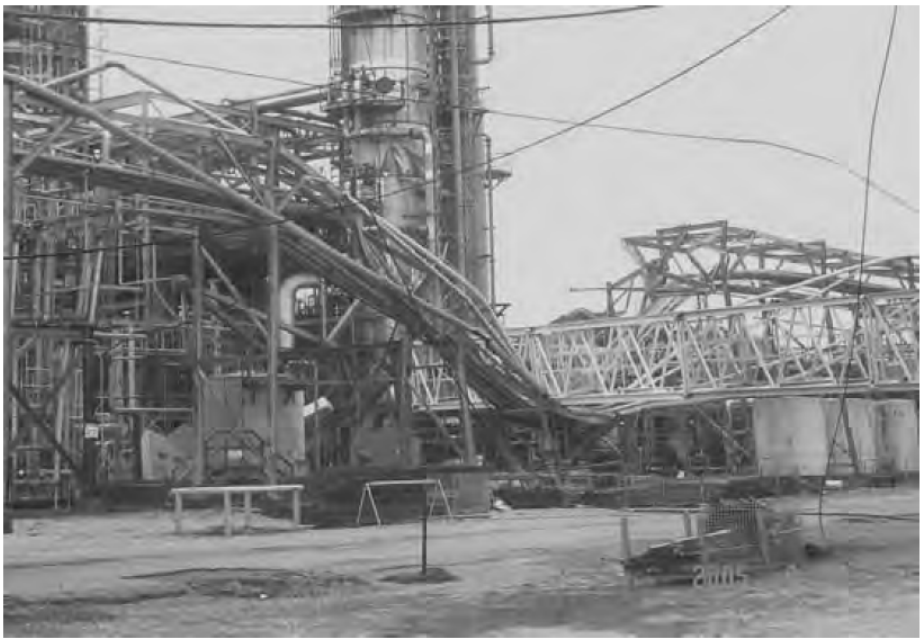

Figure 1.1: Damaged Pipe Rack - Hurricane Rita
(Photo Credit: Louisiana Chemical Association)

1.2 Review of Existing Design Practices

Before the ASCE Petrochemical Committee published the design guidelines, many of the structures commonly found in the petrochemical industry were not addressed by existing codes and standards. Due to the lack of guidelines, numerous engineers and companies within the industry had developed their own procedures and techniques for addressing various engineering issues independently. This has led to inconsistent structural reliability due to a lack of standardization in the industry. In an attempt to address this variable nature of design practices for industrial structures, the Task Committee on Wind Induced Forces and Task Committee on Anchor Bolt Design of the Petrochemical Committee of the Energy Division of ASCE published a set of guidelines for determining wind-induced forces and the design of anchor bolts for petrochemical facilities, called *Wind Loads and Anchor Bolt Design for Petrochemical Facilities* (WLABDPF) [12]. A review and discussion were conducted on thirteen design practices used to estimate wind loads on pressure vessels, pipe racks, and open structures. After the publication, the ASCE committee surveyed engineers from large engineering consulting firms to assess the level of effectiveness and acceptance of the guideline

document and determine future improvement needs. The survey showed that 21 percent of the respondents were unfamiliar with the committee report for the application of wind loads, 25 were somewhat familiar, and 54 percent were very familiar. In addition, 57 percent of the respondents referred to WLABDPF for their company specifications, while 29 percent did not refer to WLABDPF and the other 14 percent was unknown. The survey result could be summarized as 80 percent of the respondents were knowledgeable of WLABDPF, and 57 percent referenced WLABDPF in their current company design specifications. In referencing WLABDPF, it was seen that the specifications in some industrial companies had modified the tributary areas of pipes on racks, reduced wind loading on piping in a pipe rack due to multiple pipe rack levels, and used an alternative force coefficient for cable trays. Unsurprisingly, 81 percent of the respondents indicated a preference for easier-to-use methods that may provide more conservatism rather than a more detailed analysis or providing both options in the guidelines. For the improvement of future document, the ASCE committee surveyed out the structures, including arrays of structures/adjacent structures, compressor sheds, structures with dense equipment, one-bay structures, stacks, partially clad structures, cooling towers, fin fan type coolers, and pipe bridges, for which the new recommendations would benefit the associated engineers and companies the most. Out of the surveyed structures, pipe bridges had the most positive responses, with 76 percent saying it would be very beneficial and 20 percent saying it would be somewhat beneficial. As a result, the pipe bridges and pipe racks were proposed to be included in the next edition. In 2011, the ASCE committee presented an improved set of guidelines, *Wind Loads for Petrochemical and Other Industrial Facilities* (WLPOIF), which covers most structures typically seen in petrochemical facilities [15]. Recommendations and guidelines for open-frame structures and pipe racks can be found in Section 5 of WLPOIF.

Chapter 2

Literature Review

2.1 Wind Load on Structures

The wind engineering literature provides a well-documented basis and procedures for determining design wind loads for conventional structures, including enclosed structures. These design basis and procedures have been adopted and compiled by ASCE 7 [3]. Three procedures are discussed in ASCE 7 for estimating design wind loads on the main wind force resisting system (MWFRS) and on components and cladding, including envelope procedure, directional procedure, and wind tunnel procedure. These are referred to by the *International Building Code* (IBC) [10], which has been adopted throughout the United States. As the name suggests, the envelope procedure is a simplified analysis of typical regular-shaped structures. It is only applicable to relatively rigid, low-rise, and enclosed structures (i.e. without openings in the building envelope). The directional procedure is an analytical procedure that is applicable to structures of any height but limited to regular geometry and response characteristics. The wind tunnel procedure, on the other hand, is required for complex structures that are not within the limitations of the first two methods.

In addition to providing minimum load requirements for structures subjected to building codes, ASCE 7 also addresses enclosed structures, trussed towers, and simple cylinders commonly present in petrochemical facilities. On the other hand, the non-building structures, such as open-frame structures, are also addressed in ASCE 7 with further guidelines provided in the WLPOIF report [15].

This study does not discuss the selection of importance factor, gust effect factor, exposure

category, basic wind speed, and other related factors, as these are already extensively documented in ASCE 7.

2.2 Wind Tunnel Testing

ASCE 7 established several design procedures to estimate the wind loads, including the Directional Procedure and Envelope Procedure as specified in Chapters 27 and 28, respectively [3].Even though these procedures are well-defined and convenient, they are conservative and have limitations. The Directional Procedure takes into consideration the load magnification effect caused by gusts in resonance with along-wind vibrations of flexible buildings; however, it is limited to regular-shaped buildings and requires structures to be designed using recognized literature. It does not take into consideration the shielding effect, across-wind loading, vortex shedding, instability caused by galloping or flutter, or site locations with channeling effects or buffeting in the wake of upwind obstructions. In addition to the considerations and limitations discussed for the Directional Procedure, the Envelope Procedure uses the envelope approach to eliminate the wind direction parameter and is only applicable to low-rise buildings. On the other hand, ASCE 7 allows the use of wind tunnel testing to determine wind loads instead of analytical procedures [3]. The wind tunnel procedure is applicable to unusually shaped structures and provides a more accurate result. The testing requirement is briefly specified in Chapter 31 in ASCE 7, while more detailed guidance is provided in ASCE 49 [1] and ASCE Manual of Practice No. 67 [2].

2.3 Wind loads for pipe racks

The ASCE Task Committee on Wind-Induced Forces provided multiple procedures to estimate wind loads on pipe racks in the WLPOIF report [15]. These procedures are adopted from Chapter 26 of ASCE 7 for estimating design wind forces using Equation 2.1.

$$F = q_z \, G \, C_f \, A \tag{2.1}$$

Where F = applied wind force (lbs); q_z = velocity pressure (psf); G = gust effect factor (unitless); C_f = force coefficient (unitless); and A = area (ft^2) for which the force is calculated (typically projected area).

The velocity pressure, q_z, as defined by Equation 2.2, is a modification of Bernoulli's formula, which relates the flow velocity and the fluid density to the fluid dynamic pressure. The constant value of 0.00256 takes into account the density of air and a unit conversion factor. This constant is used when wind speed is expressed in miles per hour (mph), resulting in velocity pressure being expressed in pounds per square foot (psf).

$$q_z = 0.00256\, K_z\, K_{zt}\, K_d\, V^2\, I \tag{2.2}$$

Where K_z = exposure factor, K_{zt} = topographic effect factor, K_d = directionality factor, V = basic wind speeds (mph) specified by ASCE 7, and I = importance factor.

One of which procedures, provided in WLPOIF report, is to estimate wind loads using force coefficients for individual members as specified in Section 5.1 of WLPOIF [15]. Alternatively, the wind loads can be estimated using force coefficients for an open frame structure as specified in Section 5.2, Appendix 5A, and Appendix 5B. These methods are adapted from studies and testing results of Cook [7], Georgiou [8], Willford & Allsop [16], and Nadeem & Levitan [11]. One of the most commonly used cross-sections for members of pipe racks and pipe bridges are steel wide flange sections.

2.3.1 Force Coefficient of Wide Flange Section

ASCE 7 [3] and AS 1170 [6] have both published force coefficients for single-plane open frames consisting of the flat-sided member such as the wide flange section. Both organizations use the envelope approach to summarize their result. While ASCE 7 provides values with respect to the solidity ratio (ϵ) and is applicable to all wind directions, AS 1170 provides values with respect to the wind direction and is applicable to all the solidity ratios between 0.2 and 0.8. The solidity ratio (ϵ) is determined using equation 2.3. According to ASCE 7, the force coefficients for the section are provided in Figure 29.4-2 for the solidity ratio of less than 0.7 [3]. Table 2.1 shows the force coefficients with respect to the solidity ratio provided by ASCE 7.

$$\epsilon = \frac{A_e}{A_g} \tag{2.3}$$

Where A_e = projected solid area; and A_g = gross area (including openings).

Table 2.1: ASCE 7's force coefficient for flat-sided members

ϵ	**Force Coefficients,** C_f
< 0.1	2.0
0.1 to 0.29	1.8
0.3 to 0.7	1.6

On the other hand, AS 1170 published force coefficients for single-plane open frames in 1989 [6]. Most typical sections used for an open frame are included; one of which is the wide flange section whose force coefficients are provided in Table E5 of the AS 1170's Appendix E. The AS 1170 includes the wide flange section with flange width-to-depth ratios of 0.48 and 1.00. The coefficients come with two axis directions (along the flange, parallel to X-axis, and along the web, parallel to Y-axis) for wind angles of 0, 45, and 90 degrees. Table 2.2 shows the provided force coefficient with their respective parameters.

Table 2.2: AS 1170's force coefficient for flat-sided members

Depth-to-Width		**Wind direction,** θ		
Ratio		**0**	**45**	**90**
$b = 0.48d$	$C_{F,x}$	2.05	1.95	± 0.50
	$C_{F,y}$	0	-0.60	-0.90
$b = d$	$C_{F,x}$	1.60	1.50	0
	$C_{F,y}$	0	-1.50	-1.90

ASCE 7 and AS 1170 present their coefficients slightly differently; nevertheless, they have a good agreement for the maximum force coefficients of 2.00 and 2.05, respectively.

2.3.2 WLPOIF Wind Loads Procedure for Pipe Racks

The procedures for determining the wind loads for pipe racks are discussed in Section 5.1 of WLPOIF.The force coefficient for structural members of pipe racks is suggested to be 2.0 for the first level and lower and 1.6 for the higher level. Alternatively, the force coefficient of 1.8 may also be used for structural members of all levels. These values are referred from Figure 29.4.2 of ASCE 7, shown in Table 2.1. The structural area to be considered for calculating wind load should be

equal to the number of structural members multiplied by their corresponding projected area. On the other hand, the force coefficient of 0.7 should be used for the pipe members. This value is taken from ASCE 7, Figure 29.4-1, under the assumption of a moderately smooth surface with the ratio of structure's height and pipe's diameter, $h/D \geq 25$, and $D\sqrt{q_z} > 2.5$. For insulated pipes, the force coefficient for a rough pipe, which depends on the roughness coefficient of the insulation (D'/D), may be used instead where D' is the depth of protruding elements such as ribs and spoilers. The effective area of the pipes (Figure 2.1) should be equal to the sum of the maximum pipe diameter and 10 percent of the width of the bent (on which the pipes bear on) multiplied by the pipes' length, shown in Equation 2.4. This area is based on the assumption that the largest pipe is on the windward side with a wind angle of $\pm$ 5.7 degrees. The total wind load on the structure should be the total sum of all the force induced by all members, estimated using Equation 2.1.

$$A = L\ (D + 10\%\ W) \tag{2.4}$$

Where A = effective area for pipe; L = length of the pipe; D = largest pipe diameter in bent (including insulation); and W = width of the bent.

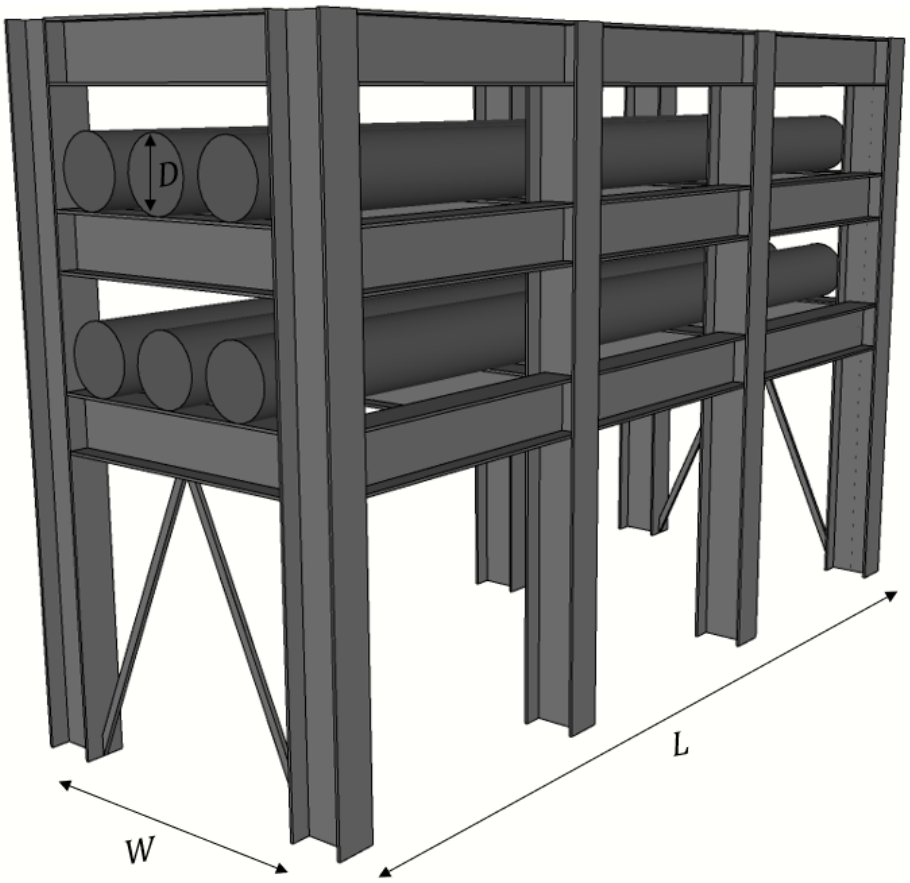

Figure 2.1: Parameters for determining the effective area of pipes

2.3.3 WLPOIF Wind Loads Procedure for Open Frame

Section 5.2 of WLPOIF shows a procedure for determining the wind loads for open frame structures. This procedure adapted the force coefficients, C_{Dg}, developed from wind tunnel tests in 1990 by Willford and Allsop for use on the gross area of structure as used by the British wind loading standard [16]. These coefficients are then converted to those that are applied to projected areas as used in ASCE 7, shown in Equation 2.5.

$$C_f = \frac{C_{Dg}}{\epsilon} \tag{2.5}$$

Where C_{Dg} = force coefficient on the gross area of the frame, taken from Figure 5.1 of WLPOIF (Fig. 2.2); and ϵ = solidity ratio of the frame.

The wind load induced by the pipe is estimated using the same approach as mentioned in Section 5.1 of WLPOIF. The total wind load on the structure should be the total sum of all the force induced by all members, estimated using Equation 2.1.

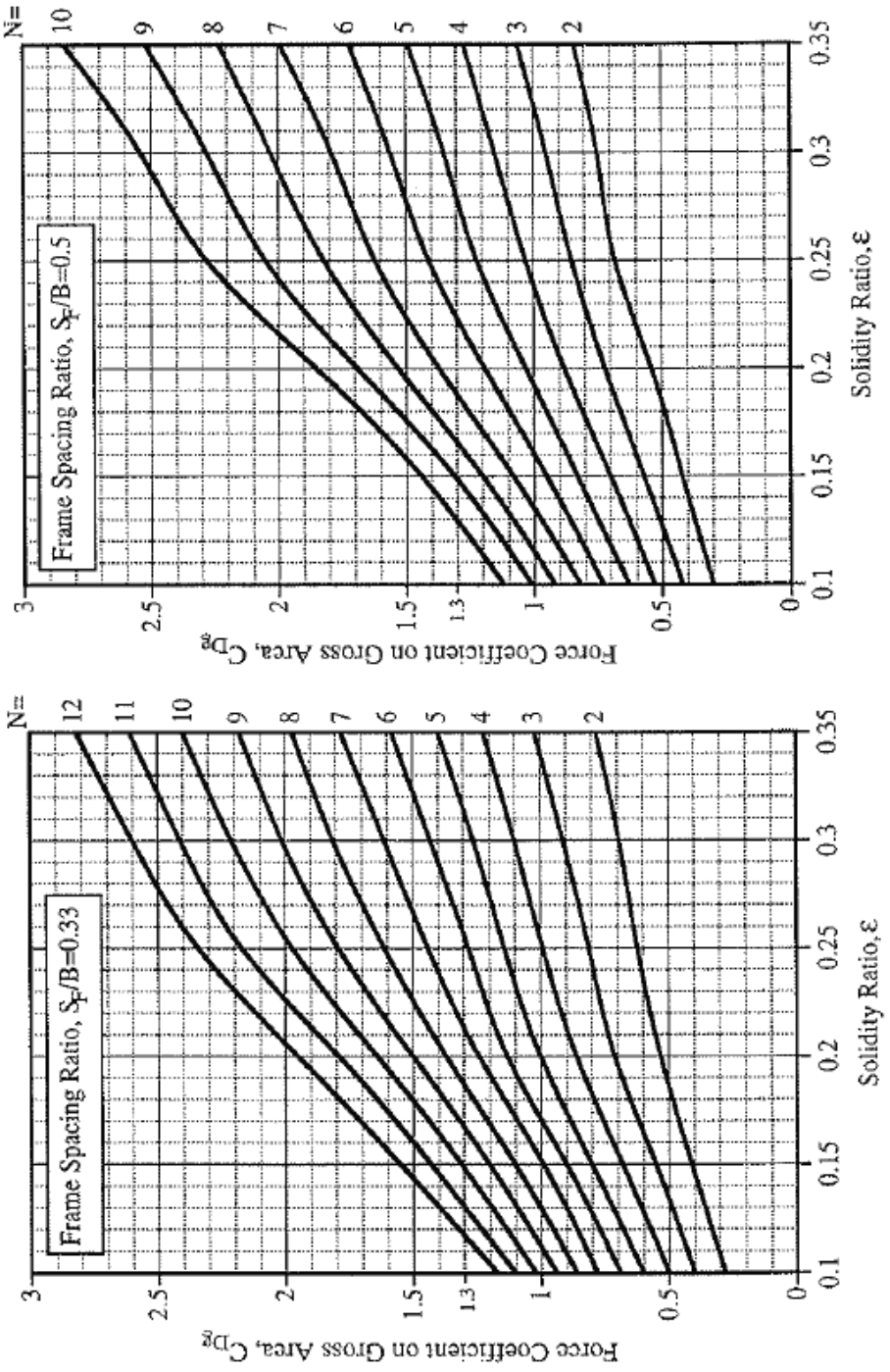

Figure 2.2: Force coefficient used in Section 5.2 of WLPOIF report

2.3.4 Alternative Procedures for Determining Force Coefficients for Open Frame

Appendix 5A of WLPOIF provides alternate methods for determining the force coefficients and load combinations of open-frame structures. In contrast to rectangular enclosed buildings, single frames, or solid signs, where maximum wind force typically occurs when the wind angle is perpendicular to the plane of interest, this is not the case for open-frame structures with multiple frames. As the wind direction deviates from the perpendicular, the columns that were once neatly aligned and shielded become staggered and exposed to the wind, and the structure's projected area normal to the wind increases.

The wind angle, which induces the maximum force along the axis of interest, can be estimated using Equations 2.6 and 2.7. The force coefficient, C_f, is taken from Figure 5A.3 of WLPOIF (Figure 2.3) and can be linearly interpolated based on the wind attack angle, α_{max}, spacing ratio, $\frac{S_F}{B}$, number of frames, N, and solidity ratio, ϵ.

$$\alpha_{max} = (10 + 58\ \epsilon)^{\circ}, \quad for \quad 3 \leq N \leq 5 \tag{2.6}$$

$$\alpha_{max} = (16 + 52\ \epsilon)^{\circ}, \quad for \quad 6 \leq N \leq 10 \tag{2.7}$$

The wind load induced by the pipe is estimated using the same approach as mentioned in Section 5.1 of WLPOIF. The total wind load on the structure should be the total sum of all the force induced by all members, estimated using the equation 2.1.

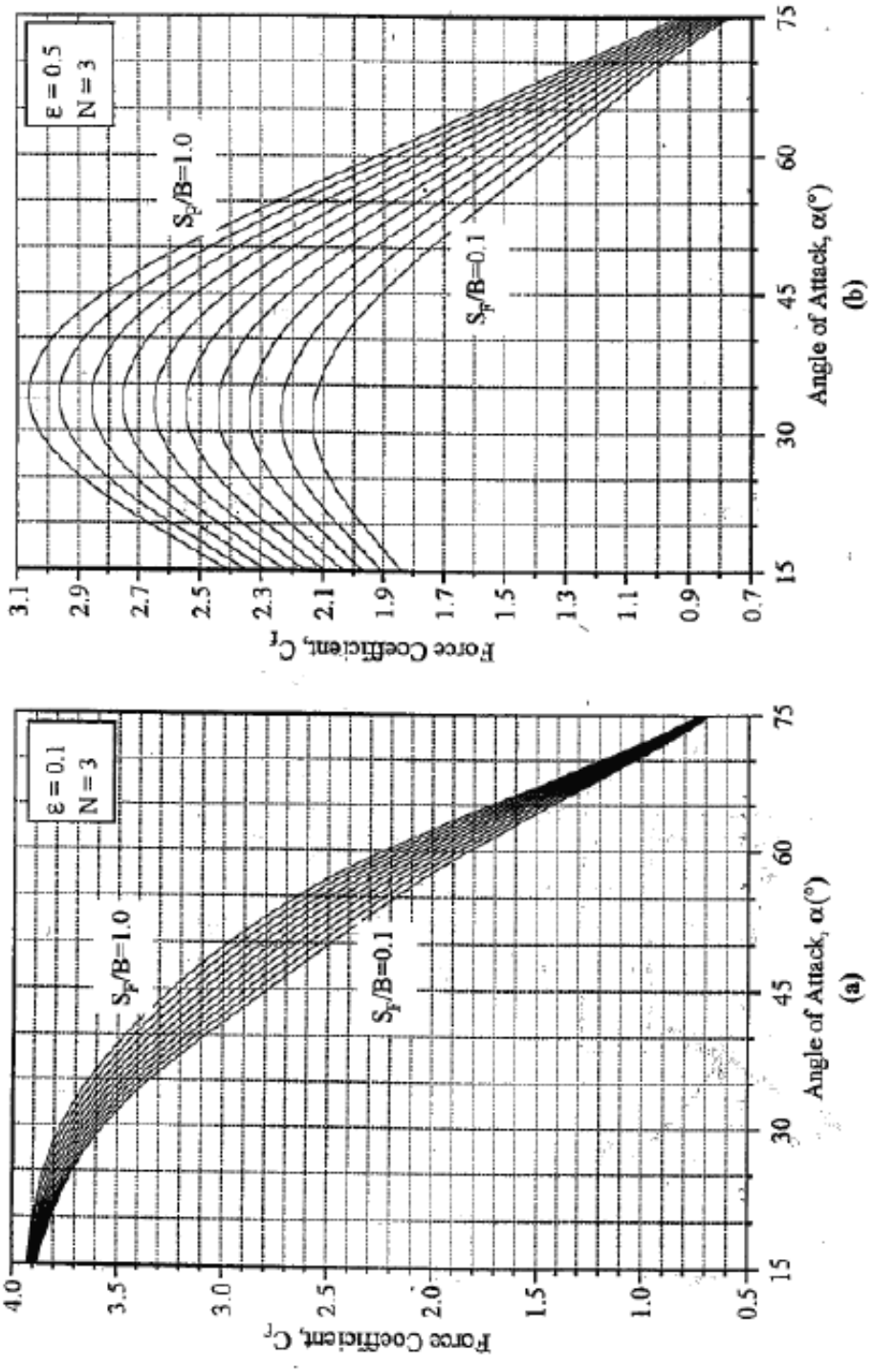

Figure 2.3: Force coefficient used in Appendix 5A of WLPOIF report

2.3.5 Wind Loads Procedure for High-Solidity Open Frame Structures

Structures with open frames frequently experience high solidity ratios beyond the values addressed in Section 5.2 and Appendix 5A of the WLPOIF report due to the positioning and crowding of structural components, piping, equipment, electrical items, and additional fixtures. As the overall structures get more densely occupied, the wind load estimation becomes much more tedious, and their accuracy may be diminished. In an attempt to tackle this issue, an analytical model developed by Louisiana State University for the force coefficient of porous structures was adapted. The maximum force coefficient for a densely occupied open-frame structure with solidity ratio of greater than 0.5 ($\epsilon > 50\%$) can be expressed in Equation 2.8. A comparison of the analytical model with wind tunnel measurements from Georgiou [8] and Qiang [14] showed a good agreement in trends, shown in Figure 2.4.

$$C_{max} = \frac{C_0 \, \phi \, \sqrt{B^2 + L^2}}{2 \, B \, (1 + \frac{B^2}{L^2} - \frac{B}{L^2} \, \sqrt{B^2 + L^2})} \tag{2.8}$$

Where C_{max} = maximum force coefficient for a densely occupied open-frame structure; C_0 = equivalent solid body force coefficient; ϕ is the total solidity ratio (including equipment); B = width of the structure; and L = length of the structure.

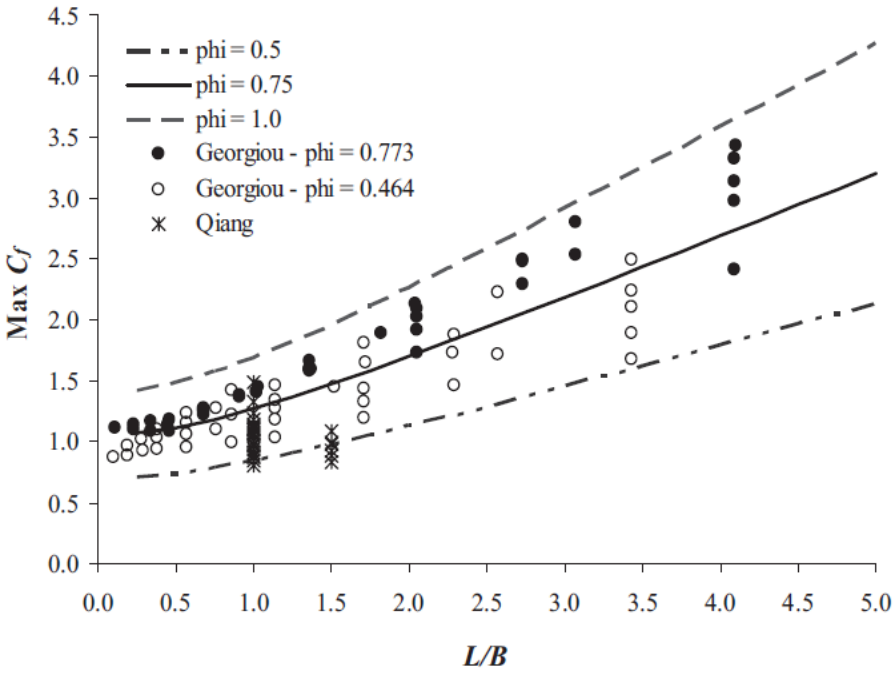

Figure 2.4: Comparison of analytical model and wind tunnel measurements. The lines indicate the results of Equation 2.8, and the points indicate wind tunnel measurements (Figure reproduced from Amoroso and Levitan, 2009 [4])

The model predicted that the force coefficient increases with the aspect ratio, and this observation was noted. As a result, it is feasible to formulate the maximum force coefficient solely based on the aspect ratio. The empirical parameter, C_0, is taken to be 1.4, which ensures that the results from the analytical model adequately envelope the force coefficient for the structures. The simplified model can be expressed in Equations 2.9 and 2.10. When applying the force coefficient, it should be used with the gross area of the structure (including openings).

$$C_f = \tfrac{1}{4}(\tfrac{L}{B})^2 + 1.4, \quad for \quad \frac{L}{B} < 1.5 \tag{2.9}$$

$$C_f = \tfrac{2}{3}(\tfrac{L}{B})^2 + 0.9, \quad for \quad \frac{L}{B} \geq 1.5 \tag{2.10}$$

Where L = along-wind length of the structure; and B = across-wind width of the structure.

Chapter 3

Force Coefficient for Wide Flange Section

The wide flange section is known for its capability to resist bending moment. Hence, there have been many applications for this optimized cross-section. It is not surprising that there have been many studies, involving the wind load on wide flange section. While there have been several publications on the force coefficients for single-plane frame and open-frame structures that utilize the wide flange section (some of which are mentioned in Chapter 2), the force coefficient for a single wide flange section is yet presented. The goal of this Chapter is to present the force coefficient for an individual wide flange section.

3.1 Experimental Test Setup

Wide flange sections (Fig. 3.1) with various flange width-to-depth ratios (b/d) were 3D printed using polylactic acid (PLA). The printed models, shown in Figure 3.1, were placed inside a wind tunnel for a force balance test in accordance with the ASCE *Manual of Practice No. 67* [2]. The wind tunnel tests for this study were conducted in the boundary layer wind tunnel at Clemson University. The wind tunnel has a cross-section of 120 in wide by 80 in high and is powered by a pair of 70 in diameter fans. The wind flow, driven by the two fans, passes through a honeycomb screen and flows across a 53 ft work section. Elements of roughness, such as roughness blocks and

spires, may be placed across the work section to generate wind flow that matches the desired type of terrain and model scale. For this study, no element of roughness is used since uniform wind flow is preferred for estimating the force coefficients. A total of five wide flange sections with a flange width to depth ratios of 1.0, 0.9, 0.7, 0.5, and 0.3 are tested in the wind tunnel for angles from 0° to 90° with 10° increments. In addition, the angle of 45° is also tested to compare with the values from AS 1170 for verification purposes. It is assumed that the other quarters yield similar results due to symmetrical geometry of the wide flange section. The force measured in the two principal directions (X and Y axes, Fig. 3.2), F_i, were used to determine the force coefficients, C_i, using Equation 3.1.

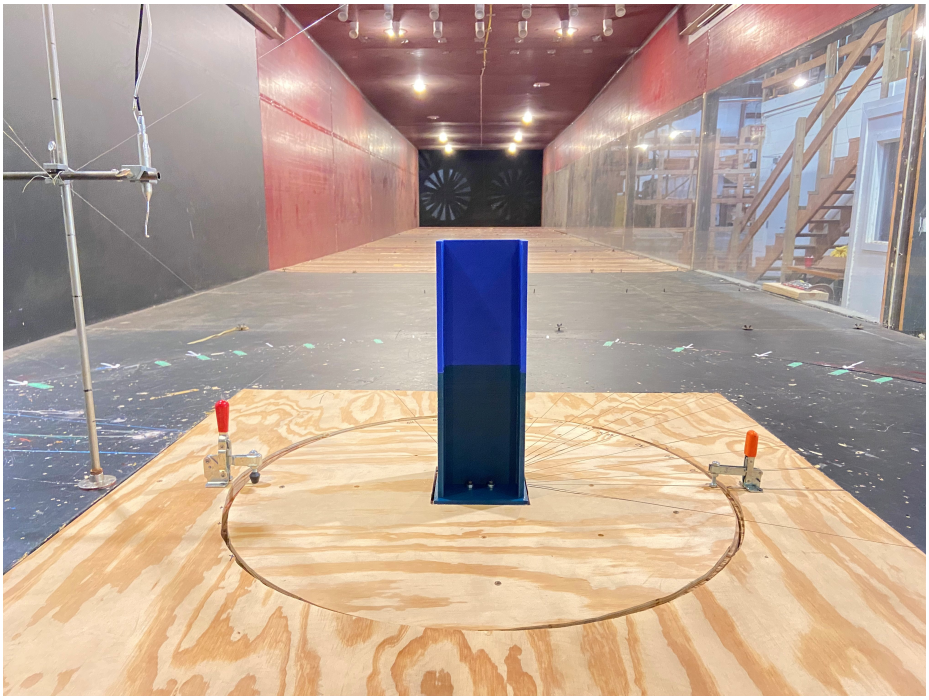

Figure 3.1: Experimental setup for wide flange section

$$F_i = \frac{1}{2}\,\rho\,V^2\,A_\alpha\,C_i \tag{3.1}$$

Where ρ = air density; V = wind velocity; and A_α = projected area at wind attack angle α (Eq. 3.2).

$$A_\alpha = A_0\,(cos\alpha + r\ sin\alpha) \tag{3.2}$$

Where α = wind attack angle; r = flange width to depth ratio; and A_0 = projected area normal to the wind direction at the attack angle of 0°.

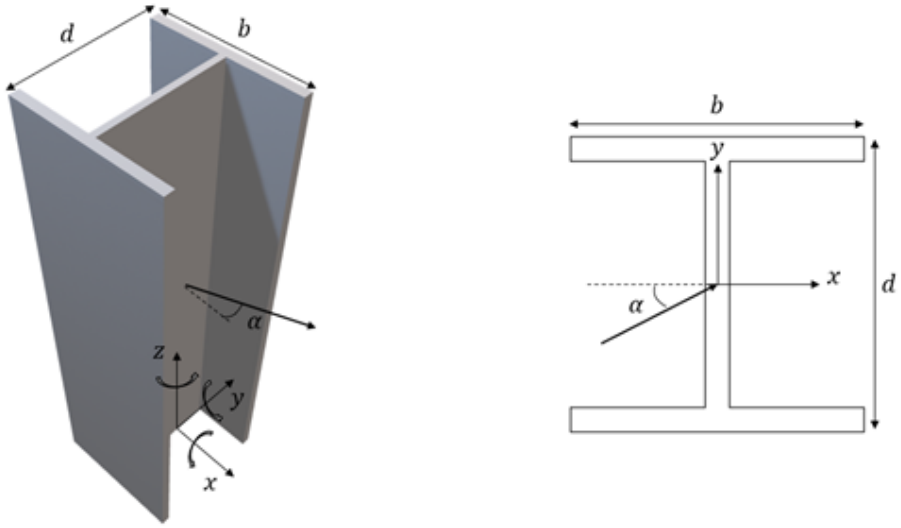

Figure 3.2: Isometric and plan view for wide flange section model

3.1.1 Wind Profile

The wind velocity for this study is measured using a cobra probe. As mentioned in Section 3.1, the wind velocity profile is measured without the element of roughness as shown in Figure 3.1. Figure 3.3 shows the velocity profile for the wind flow measured during this study. The measured wind velocity is curve-fitted using a model (Eqn. 3.3), proposed by Hellman (1916). This test setup yields a power-law exponent, $\frac{1}{\alpha}$, of 0.123 for a geometric scaling of 1:15, which is reasonably close to Davenport's (1960) power-law exponent of 0.15 for open flat terrain (exposure C).

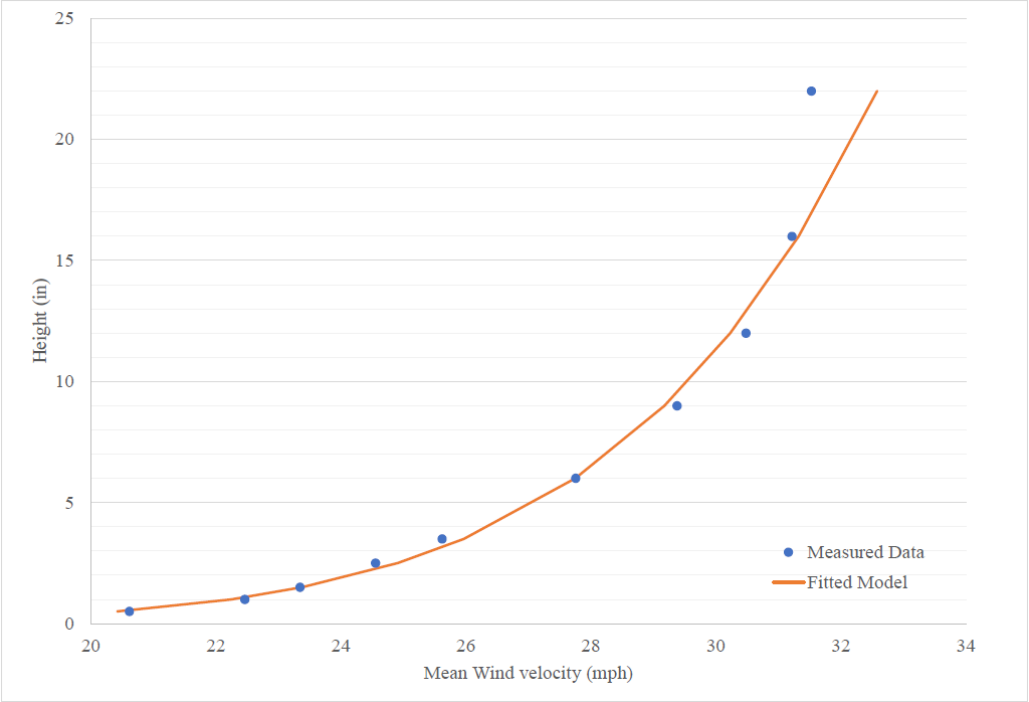

Figure 3.3: Wind velocity profile

$$\frac{V(z)}{V(z_r)} = \left(\frac{z}{z_r}\right)^{\frac{1}{\alpha}} \tag{3.3}$$

Where V(z) = wind velocity measured at height z; $V(z_r)$ = wind velocity measured at reference height z_r; and $\frac{1}{\alpha}$ = power-law exponent.

Since uniform wind flow is assumed for the force coefficients of the wide flange for this study, a correction is applied for the difference induced by the profile measured, shown in Figure 3.4. The forces measured are scaled by a correction factor, S (Eq. 3.4).

$$S = \frac{F_U}{F_N} \tag{3.4}$$

Where F_U = total force acted on the column due to an ideal uniform wind velocity measured at the height of the column; and F_N = total force acted on the column due to actual wind velocity profile measure in the wind tunnel.

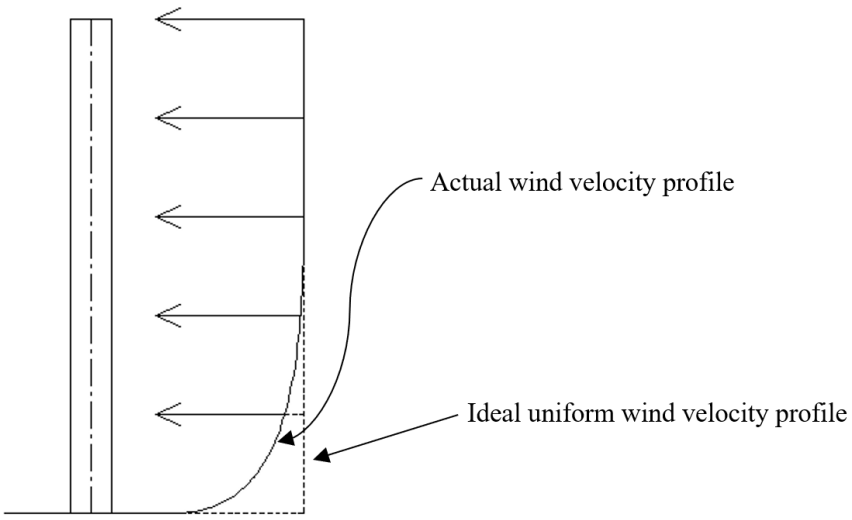

Figure 3.4: Actual wind velocity vs. ideal uniform wind velocity profile

The integral length scale of turbulence is a measurement of the separation distance over which the eddy velocities at two distinct points are correlated. Based on Taylor's hypothesis, the longitudinal integral length scale can be expressed as Equation 3.5.

$$L_u^x = \frac{\bar{U}}{\sigma_u^2} \int_0^\infty R_u(\tau)\, d\tau \tag{3.5}$$

Where $\bar{U}$ = longitudinal mean wind velocity; σ_u = standard deviation of the longitudinal wind velocity; and $R_u(\tau)$ is the auto-correlation function of longitudinal wind velocity fluctuation.

The wind fluctuations and distribution of turbulence are often described using Von Karman's power spectrum,$S_u(n)$, as shown in Equation 3.6.

$$S_u(n) = \frac{2\,\sigma_u^2\,L_u^x}{\bar{U}\,[1 + 2\,(2\,c\,n\,L_u^x\,/\,\bar{U})^2]^{5/6}} \tag{3.6}$$

Where c = 2.5; and n = natural frequency.

For ideal wind simulation, the integral length scale should be scaled properly based on the geometric scale. However, the determination of the length scale is not necessary for this study since a uniform flow is preferred over a simulation of a particular turbulence flow.

3.2 Result and Discussion

A result of force coefficients for wide flange sections with b = 1.0d, and b = 0.5d are used to compare with the force coefficients provided by AS 1170. As mentioned in Section 2.3, the provided force coefficients were obtained from an experimental test for a single-plane open frame. Even though the test setup for this study is different, the values from AS 1170 can be used to verify that the conducted tests yield reasonable results. The comparisons for wide flange sections with b = 1.0d, and b = 0.5d are shown in Figures 3.5 and 3.6 respectively. It is concluded that the tests yield meaningful results since the trend lines of the force coefficients obtained from this study match those provided by AS 1170, and the values are somewhat similar. The offsets between the AS 1170 trend lines and those of this study are likely attributed to the differences in test setups. The force coefficients of this study were obtained from a single cantilever wide flange section while those of the AS 1170 were based on a single plane open frame.

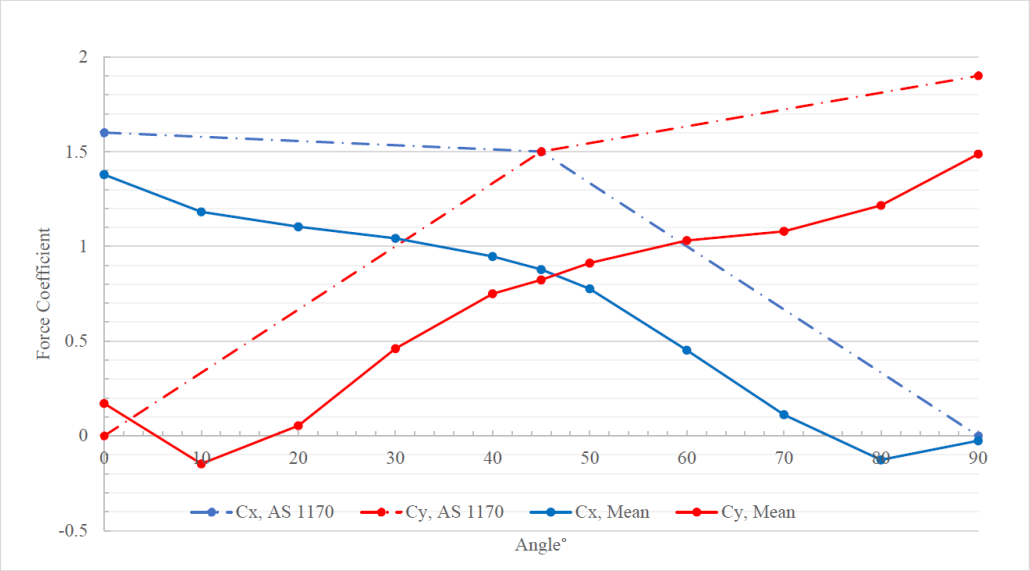

Figure 3.5: A comparison of force coefficients for wide flange section with b = 1.0d

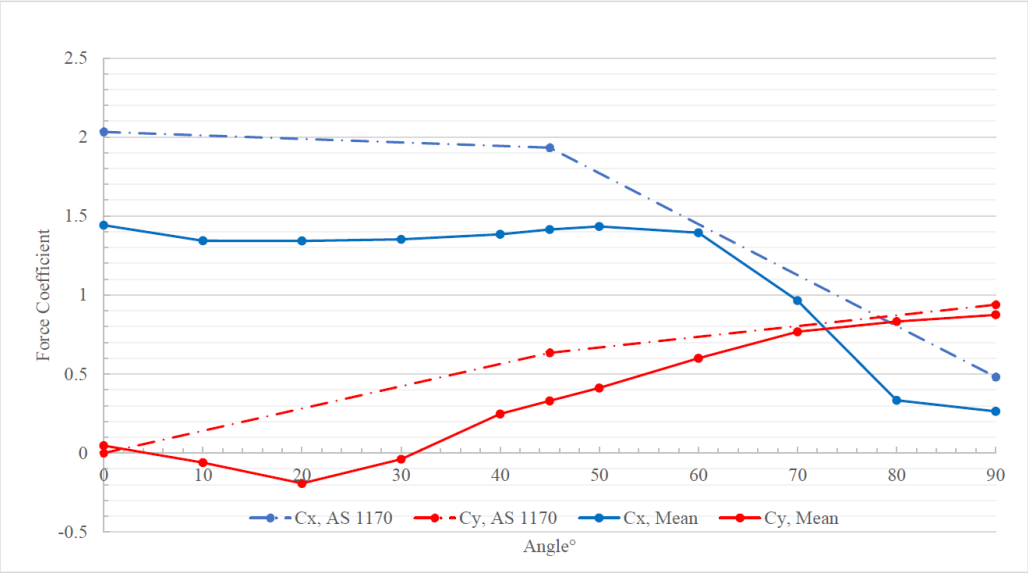

Figure 3.6: A comparison of force coefficients for wide flange section with b = 0.5d

A summary results of the mean force coefficients for all wide flange sections are shown in Tables 3.1 and 3.2. Along the X axis, it is as expected that the maximum force coefficient occurs when the axis is parallel to the wind direction at an angle of 0° with the exception of the wide flange section with b = 0.3d which peaks at an angle of 70°. Similarly, the force coefficients along the Y axis peak at 90°. A graph assuming linear behavior between angles for all the sections is shown in Figure 3.7. It is also shown that the test result falls below the recommended values from ASCE 7, mentioned in Section 2.3, except for the maximum coefficient, C_x, for the wide flange section with b = 0.3d at 70°, which falls within the recommended values (base on the solidity ratio, ϵ).

Table 3.1: A summary result of the force coefficients along the X Axis for wide flange section, C_x

Width-to-	Angle°										
Depth Ratio	0	10	20	30	40	45	50	60	70	80	90
b = 1.0d	1.38	1.18	1.10	1.04	0.95	0.88	0.78	0.45	0.11	-0.13	-0.03
b = 0.9d	1.36	1.20	1.13	1.10	1.03	1.00	0.92	0.63	0.26	0.01	0.10
b = 0.7d	1.49	1.37	1.31	1.27	1.28	1.27	1.23	0.94	0.40	-0.07	0.05
b = 0.5d	1.44	1.34	1.34	1.35	1.38	1.42	1.43	1.39	0.96	0.33	0.26
b = 0.3d	1.43	1.35	1.39	1.43	1.48	1.53	1.60	1.71	1.79	1.03	0.46

Table 3.2: A summary result of the force coefficients along the Y Axis for wide flange section, C_y

Width-to-	Angle										
Depth Ratio	0	10	20	30	40	45	50	60	70	80	90
b = 1.0d	0.17	-0.15	0.05	0.46	0.75	0.82	0.91	1.03	1.08	1.22	1.49
b = 0.9d	0.15	-0.14	-0.03	0.36	0.63	0.69	0.79	0.94	0.99	1.09	1.33
b = 0.7d	0.01	-0.06	-0.20	0.25	0.58	0.68	0.77	0.99	1.12	1.26	1.48
b = 0.5d	0.05	-0.06	-0.19	-0.04	0.25	0.33	0.41	0.60	0.77	0.83	0.87
b = 0.3d	-0.01	-0.04	-0.03	-0.10	0.14	0.23	0.29	0.47	0.71	0.97	1.39

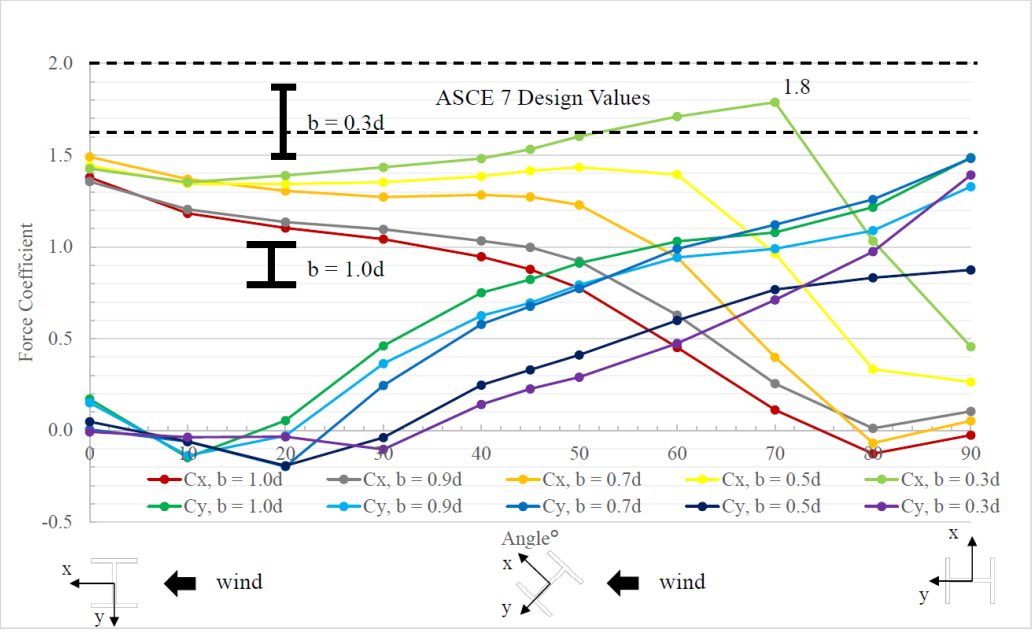

Figure 3.7: Force coefficient for wide flange sections

Chapter 4

Wind Load for Pipe Racks

Retrofitting existing pipe racks can often save on cost and time compared to constructing new ones. However, there are no clear design codes and guidelines to estimate wind loads on retrofitted pipe racks. The objective of this study is to present a series of force coefficients for the proposed retrofit strategy and discuss whether the existing design methods are applicable to the retrofitted pipe racks. The force coefficients are determined using the force balance test inside a wind tunnel.

4.1 Experimental Test Setup

A two-story pipe rack prototype (Fig. 4.1) was selected for this study. The pipes, carried by the rack, vary in two sizes. The small pipes have a scaled diameter of 1 foot, while the larger ones have a scaled diameter of 3 feet. Similar to the wide flange model, a scaled model of 1:15 was 3D printed. The 3D printed pipe racks model is then placed inside a wind tunnel for a force balance test, shown in Figure 4.2, in accordance with the ASCE Manual of Practice No. 67 [2]. The configuration for the wind velocity profile is identical to that mentioned in Section 3.1.1. The wind attack angles of 0° to 90° with 10° increments are investigated. As mentioned in Section 3.1, only a quarter of the wind attack angles are necessary for testing since the other quarters should yield similar results due to symmetry. The force coefficients, C_i, for the pipe racks are determined using Equation 4.1.

$$F_i = \frac{1}{2}\,\rho\,V^2\,A_0\,C_i \tag{4.1}$$

Where A_0 = projected area at wind attack angle of 0°.

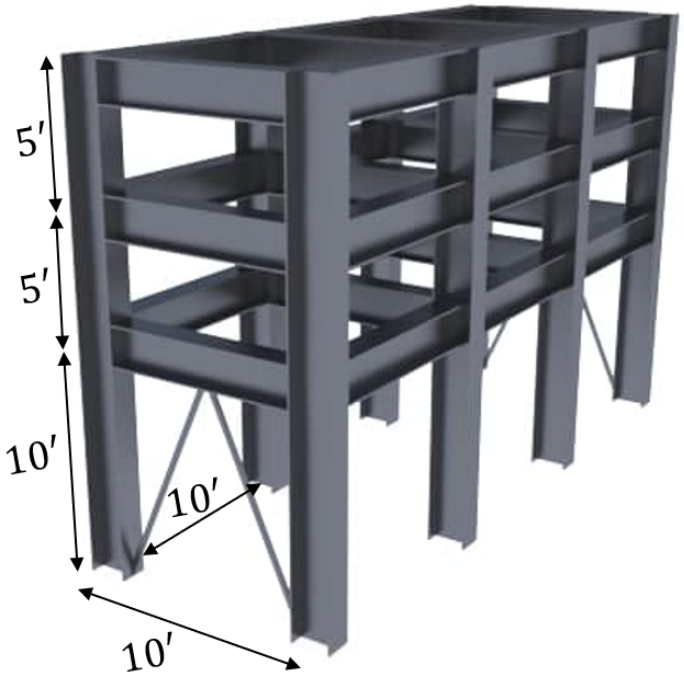

Figure 4.1: Isometric view of pipe rack prototype

Figure 4.2: Test setup for pipe rack's force balance test

In existing pipe racks, extenders may be added as short cantilever beams to accommodate additional pipes. A series of force balance tests are conducted on the various configurations, shown in Figure 4.3. A total of 5 configurations for pipe rack retrofit are investigated, shown in Figure 4.5. For verification purpose, the bare frame of the pipe rack model is also tested, shown in Figure 4.4. In addition, a few pipe configurations were investigated to see if the arrangement of pipes would influence the aerodynamic response of the structure.

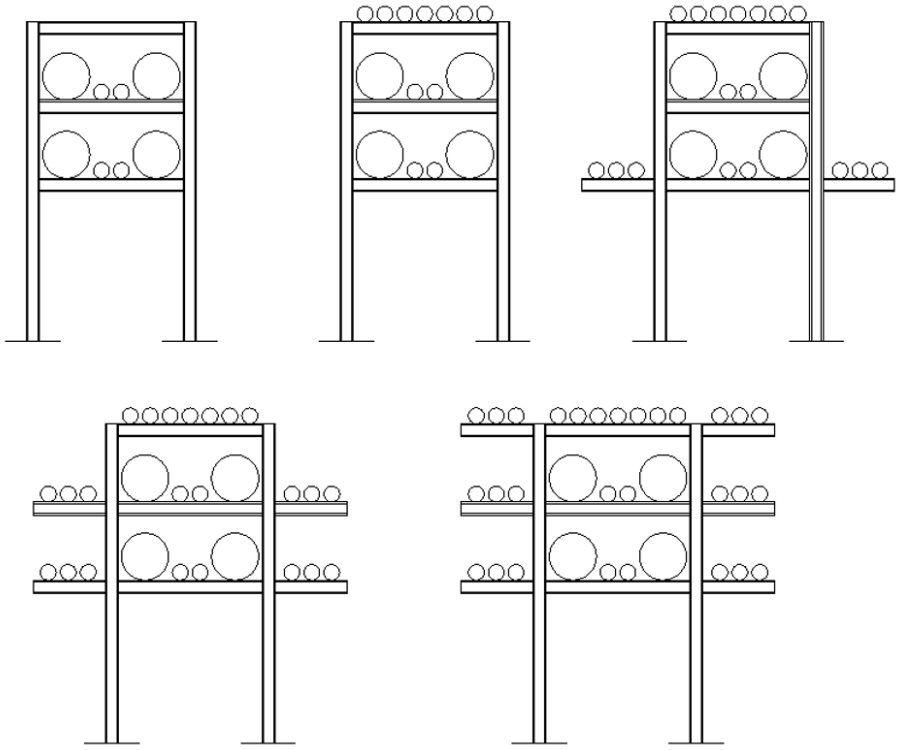

Figure 4.3: Configurations for pipe rack retrofit

Figure 4.4: Bare frame of pipe rack

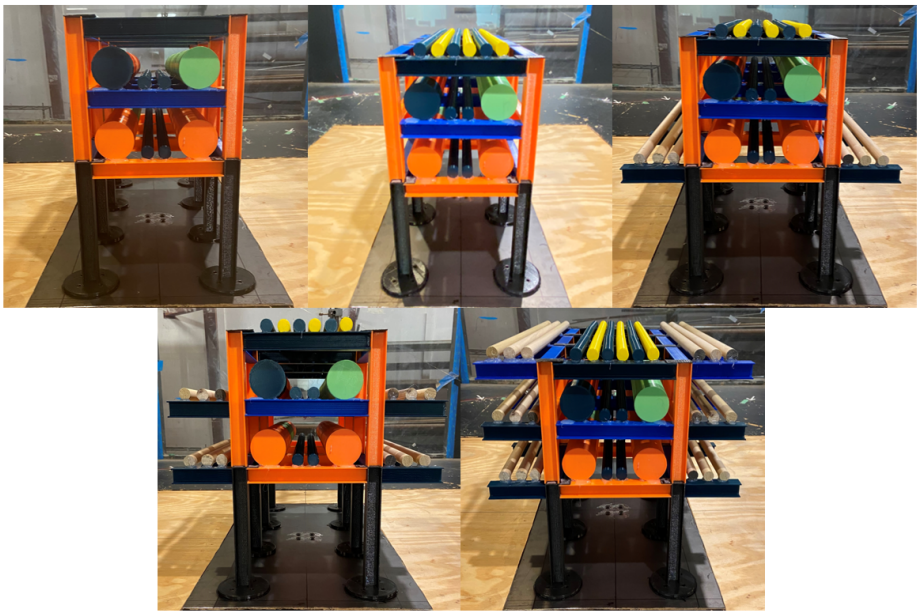

Figure 4.5: Configurations for pipe rack retrofit

4.2 Result and Discussion

The base shear, measured when the wind direction is normal to the model frame (at 0° angle), is used to compare with the expected base shear, estimated using the method reviewed in Section 2.4. All the approaches mentioned in Section 2.4 are used except for the one discussed in Section 2.4.3 since it is only applicable for the number of frames between 3 and 10. The comparison is shown in Figure 4.6. The measured base shear for configuration 0 (bare frame) has very good agreement with the value estimated using Section 5.2 of the WLPOIF report, which makes sense since this method was developed from a wind tunnel study for open-frame structures, such as the tested bare frame model. Even though the method discussed in Section 5.1 of the WLPOIF report shows an underestimation for the bare frame, all the methods discussed in this study have a similar trend. The methods discussed in Sections 5.1 and 5.2 of the WLPOIF report produce a very reasonable result, while the method discussed in Appendix 5B of the WLPOIF report shows quite an overestimation. This is reasonable since the method in Appendix 5B is developed for open-framed structures with high solidity ratio of more than 50 percent; however, it can be utilized for a quick and easy estimation of wind loads.

In addition, the force coefficients from Tables 3.1 and 3.2 are used to estimate the model base shear with the procedure discussed in Section 5.1 of the WLPOIF, shown in Figure 4.6. The result shows an underestimation since these coefficients were obtained from testing a single wide flange column and do not consider the effect of any column lines behind the first one. However, it follows a similar trend and falls within a reasonable range.

Looking at the measured base shear, it is expected that the load increases as more pipes are added, with the exception of configuration 4, which shows a slight drop in the load. This is likely due to the aerodynamic response of this particular configuration. It is suspected that the additional pipes help the wind flow around the inter-stories rather than through the inter-stories and therefore reduce the drag force on the model. In an attempt to investigate this, the pipes were re-arranged, and additional tests were conducted. The test results are shown in Figure 4.7. The additional pipes on the top cantilevers of configuration 5 are removed to allow easier flow around and above the inter-stories. As expected, there was a drop in the wind load due to a larger portion of wind flow bypassing the inter-stories. To amplify this effect, the front two small pipes on the second story are replaced with a larger pipe, so that the smooth curved surface of the larger pipe would further block

the inter-story and redirect the flow around it. The result yields a larger drop in wind load, just as expected. Finally, a larger pipe is used to replace two smaller pipes on the third story, similar to the second story, to add blockage to this flow behavior and make it harder for the wind to flow around and above the structure. As anticipated, there was an increase in wind load. Further investigation on the flow separation and envelope are required to further support this hypothesis.

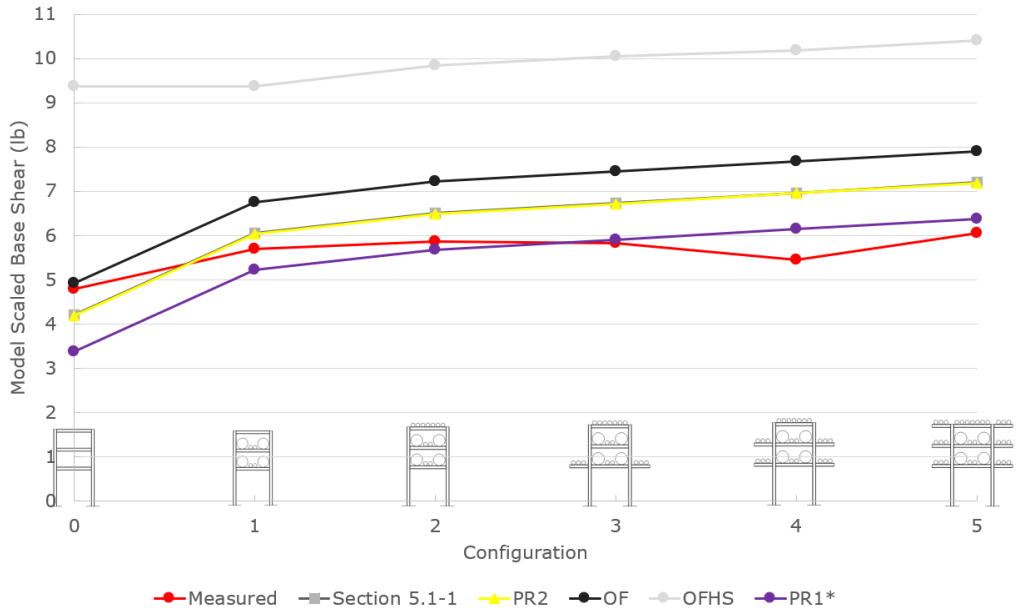

Figure 4.6: A comparison of result for model base shear with existing approaches. PR1: Section 2.3.2 with $C_f = 2.0$ for structural members on the first level and 1.6 for the higher level. PR2: Section 2.3.2 with $C_f = 1.8$ for structural members. OF: Section 2.3.3. OFHS: Section 2.3.5. PR1*: Section 2.3.2 with C_f obtained from Table 3.1 and 3.2

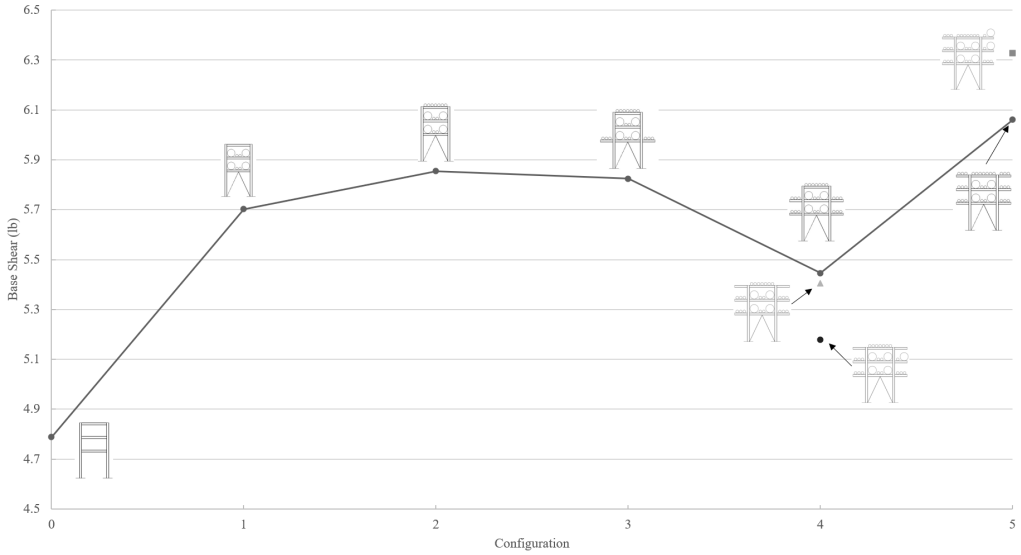

Figure 4.7: A comparison of result for model base shear with different pipe configurations

The measured force coefficients for configurations 0, 1, 2, 3, 4, and 5 are shown in Figure 4.8 through Figure 4.13 respectively. It appears that the force coefficients peak at roughly 20° and 70° with the exception of configuration 1, which peaks at 30°. As mentioned in Section 2.4.3, this is because as the wind moves away from the normal, more area gets exposed to the wind while the projected area normal to the wind also increases. Figures 4.17 and 4.18 show how the structural elements nicely line up and create the shielding effect while Figures 4.19 and 4.20 show that more structural elements get exposed to the wind as the wind moves away from the normal. This behavior is also discussed in Appendix 5A of the WLPOIF report. A summary result of the measured force coefficients along the X axis and Y axis is shown in Figures 4.14 and 4.15, respectively. It is shown in Figure 4.16 that the resultant force angle deviates from the wind angle, which is likely caused by the aerodynamic behavior of the wide flange section. The maximum angle deviation occurs at 30° with a maximum deviation of 16° for configuration 1. However, this effect becomes less pronounced as the solidity ratio increases.

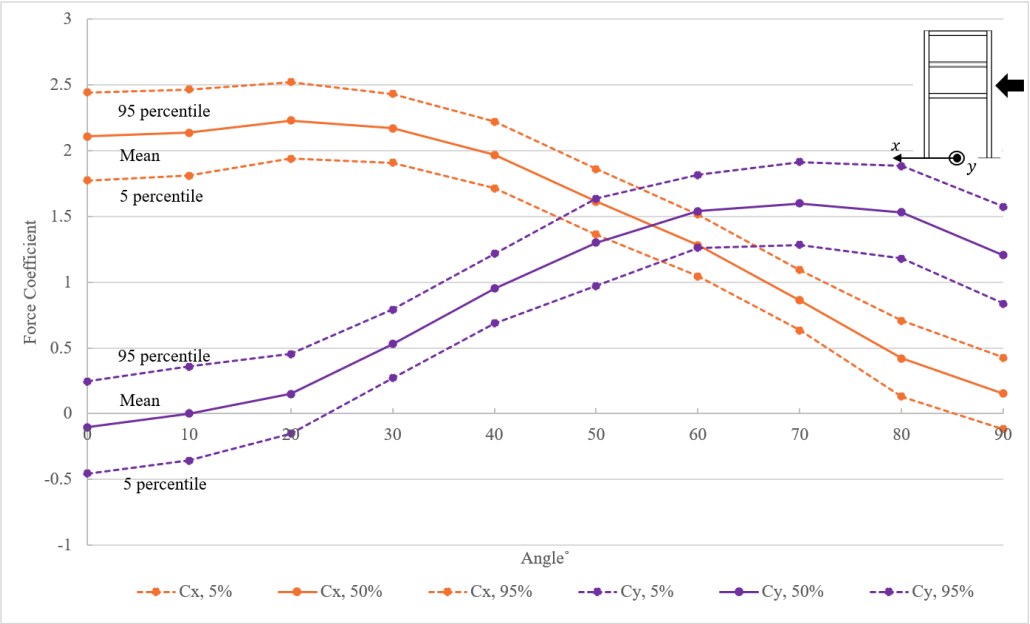

Figure 4.8: A summary result of force coefficients for configuration 0

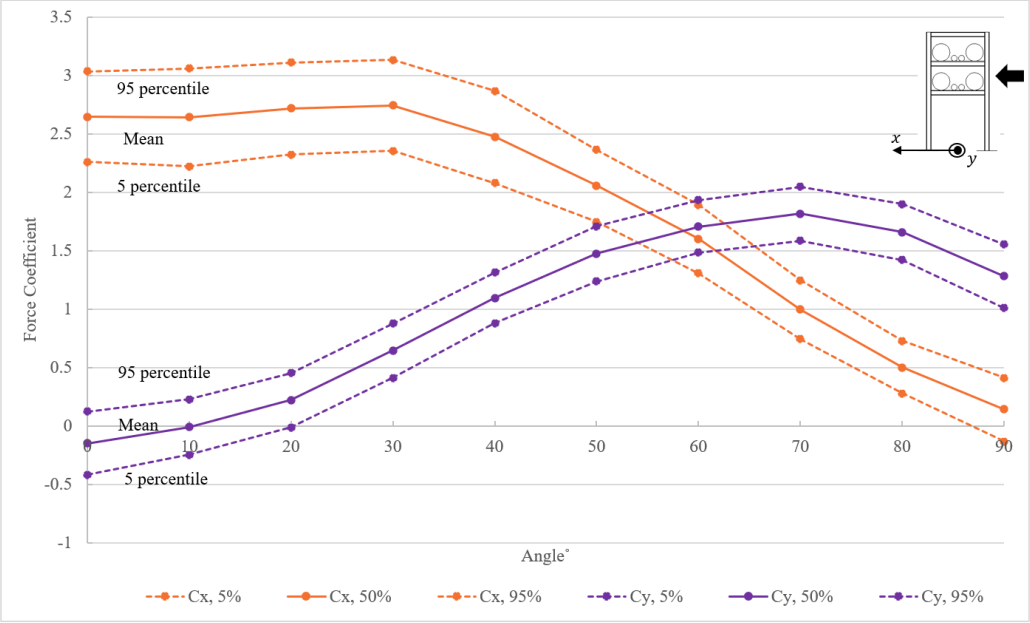

Figure 4.9: A summary result of force coefficients for configuration 1

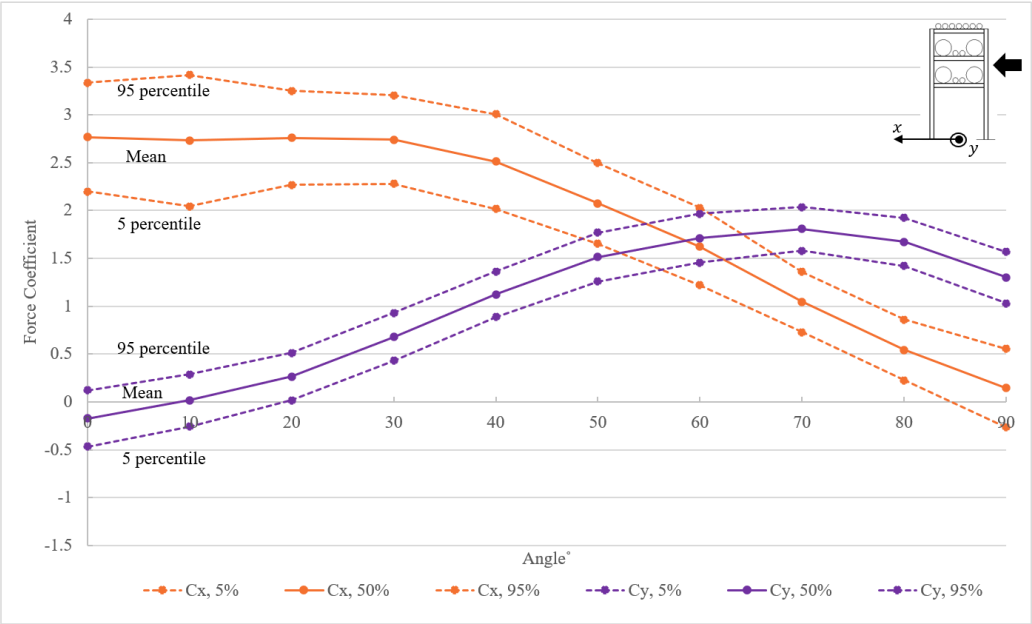

Figure 4.10: A summary result of force coefficients for configuration 2

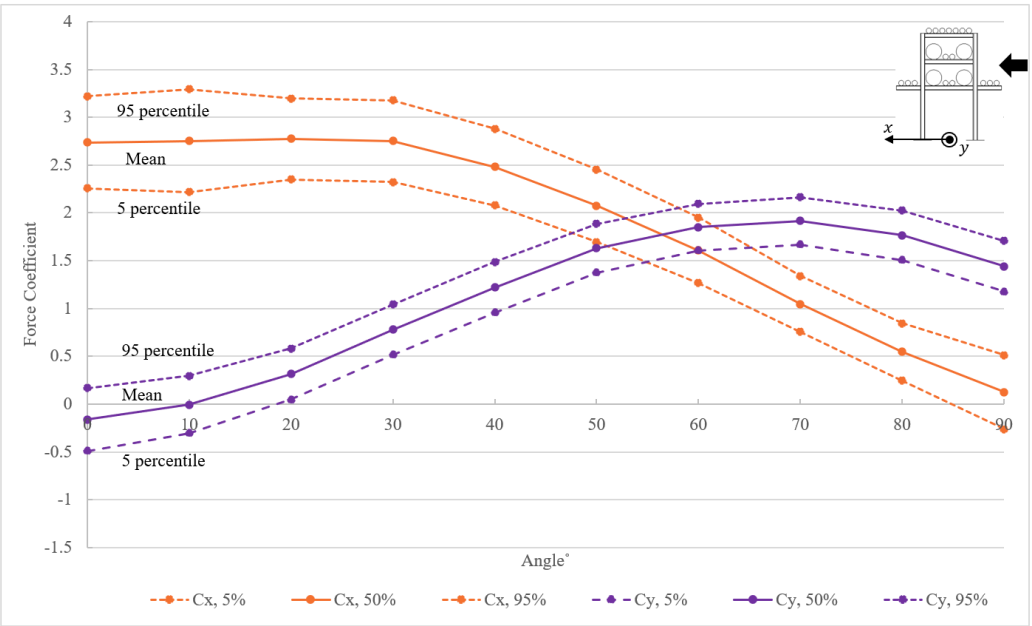

Figure 4.11: A summary result of force coefficients for configuration 3

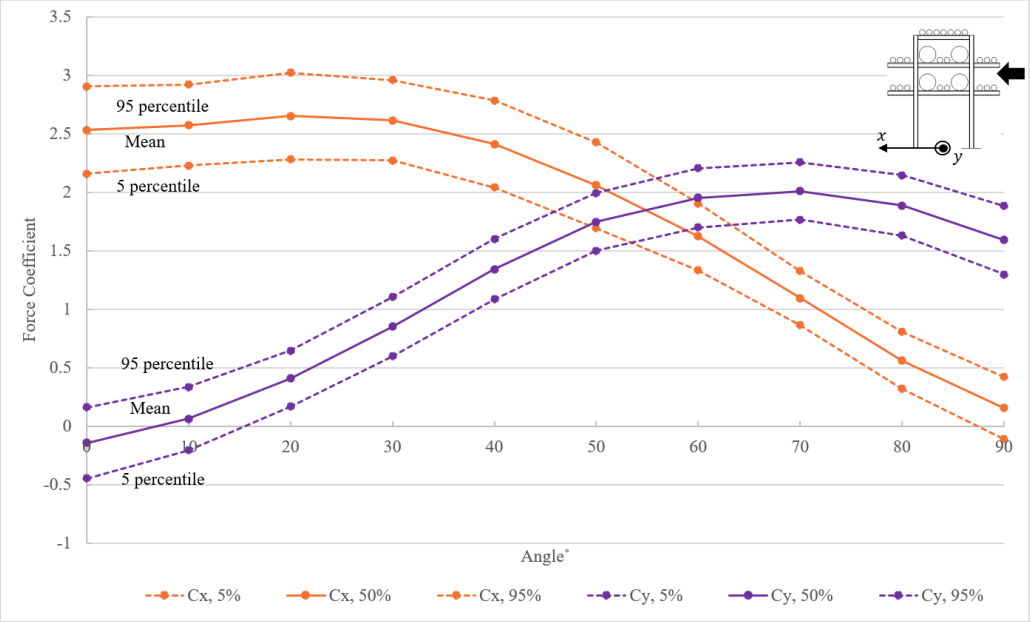

Figure 4.12: A summary result of force coefficients for configuration 4

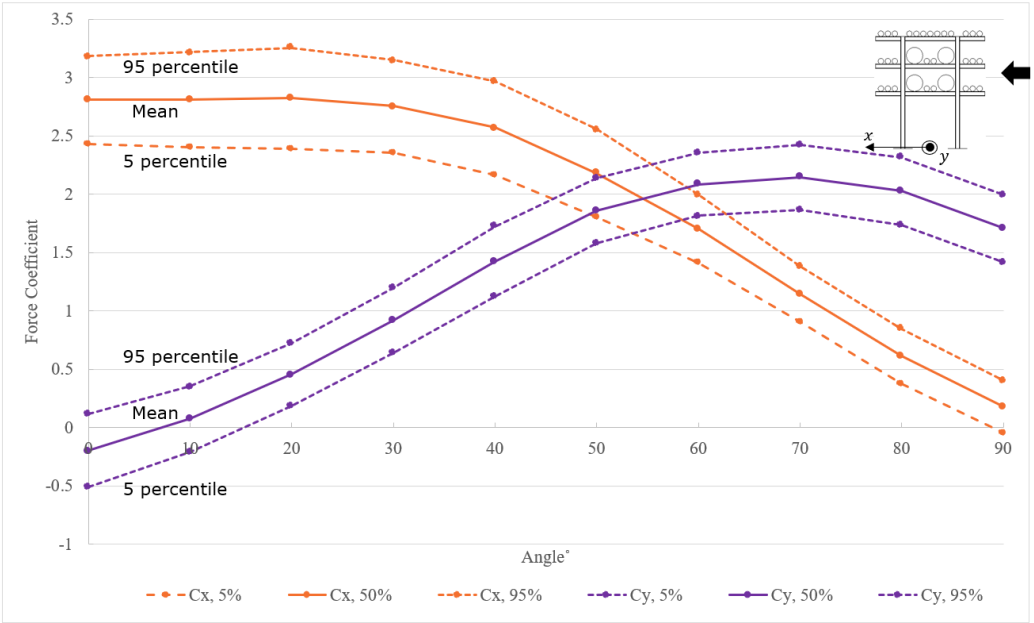

Figure 4.13: A summary result of force coefficients for configuration 5

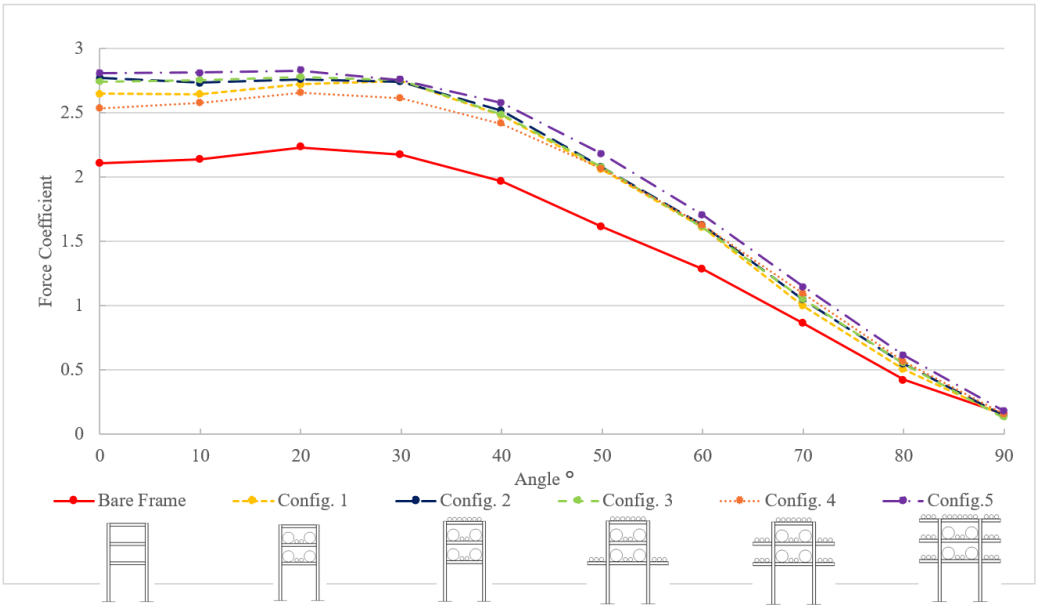

Figure 4.14: A summary result of force coefficients along X axis

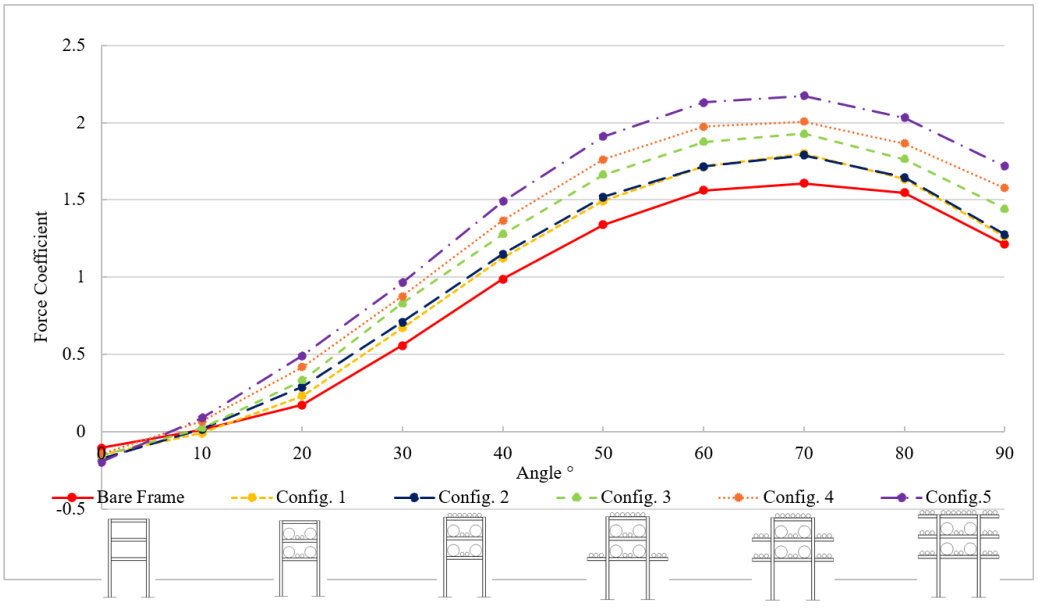

Figure 4.15: A summary result of force coefficients along Y axis

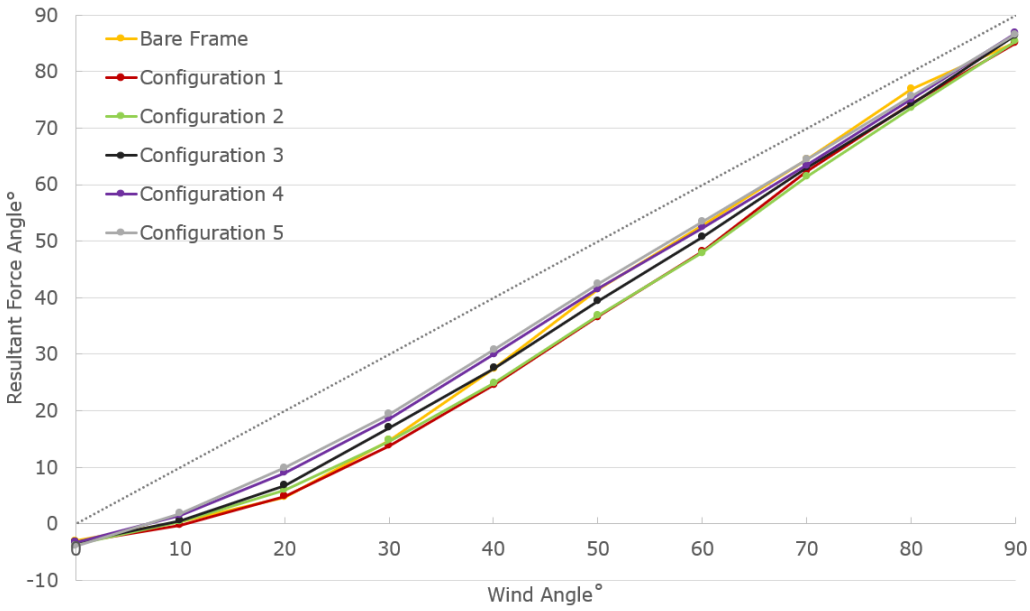

Figure 4.16: Resultant force angle

Figure 4.17: Pipe rack model at 0° angle

Figure 4.18: Pipe rack model at 30° angle

Figure 4.19: Pipe rack model at 60° angle

Figure 4.20: Pipe rack model at 90° angle

Chapter 5

Load Re-Distribution Due to Column Losing its Capacity

In industrial facilities, it is not uncommon to see existing pipe racks and other structures. There have been cases where the structural steel members are in bad enough condition that they are unlikely to provide sufficient load resistance. A commonly seen cause is corrosion, as shown in Figure 5.1. Therefore it is reasonable to assume that the steel member would lose its load-carrying capacity during extreme wind events. For this study, a column is detached from the support to investigate the load re-distribution within the pipe rack model.

Figure 5.1: Corrosion issue of a steel structural member

5.1 Experimental Test Setup

The same pipe rack model used in configuration 5 of the tests discussed in Chapter 4 is also used for this investigation. Firstly, each column's base shear is measured for the model before the column loses its capacity (pre-column detachment model), shown in Figure 5.2. A column, namely D2, is then cut off for a re-measurement which leaves a total of 7 columns that are still attached to supports (post-column detachment model), as shown in Figure 5.3.

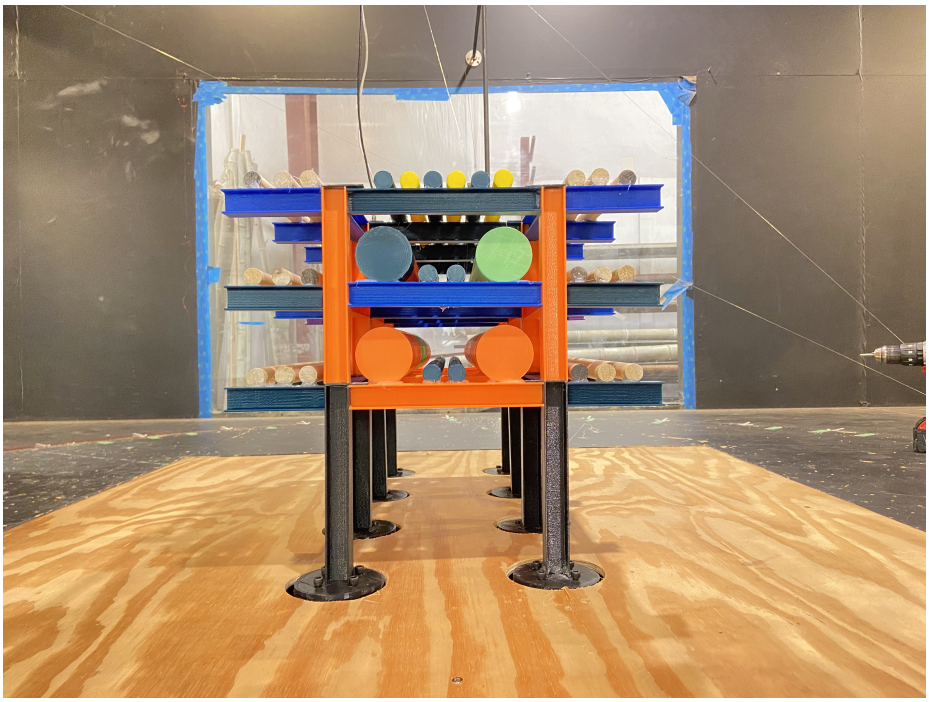

Figure 5.2: Pre-column detachment pipe rack model used to investigate load re-distribution

Figure 5.3: Post-column detachment pipe rack model used to investigate load re-distribution

A total of four load cells, capable of measuring forces and moments for all three axis directions, are utilized to measure the base shear of four attached columns. The axis direction for measurement is shown in Figure 5.5. The test is done twice with load cells (Fig. 5.4) being alternated to the other columns.

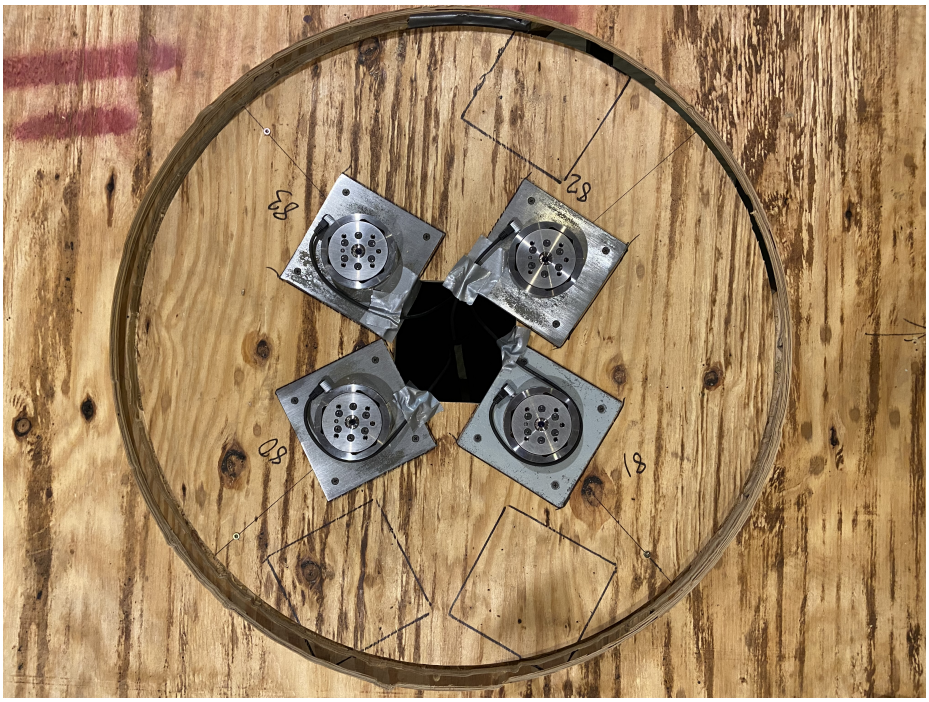

Figure 5.4: Load cells used to measure base shear of the attached columns

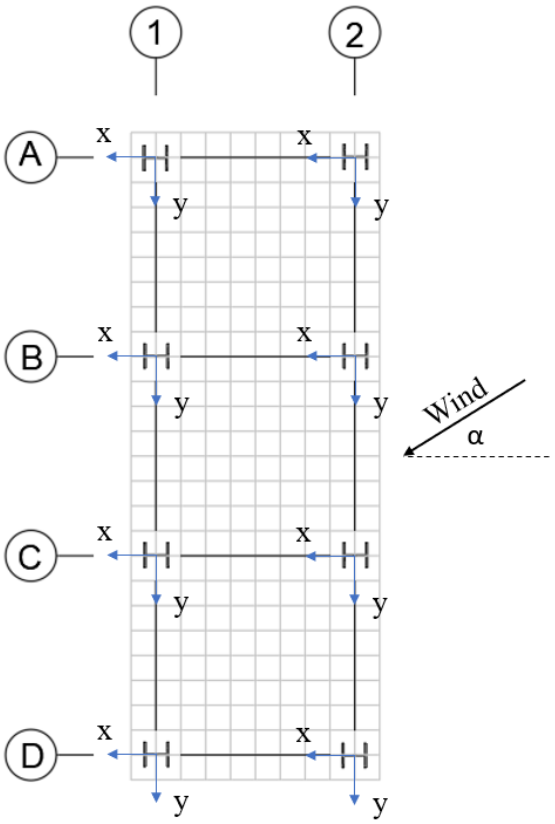

Figure 5.5: Axis direction for test measurement

5.2 Result and Discussion

The base shear of each column measured from the pre-column detachment model is summed up to compare with the total base shear measured during testing discussed in Chapter 4. Figure 5.6 shows the comparison along the X-axis and Y-axis as well as the resultants. This graph proves that multiple testings with alternating load cells do not produce any impacting variation and should yield similar results as if one load cell were used to be placed under each column for a single test. In other words, the sum of forces measured by load cells at each individual column equals the force on a single load cell measuring the force on the entire frame.

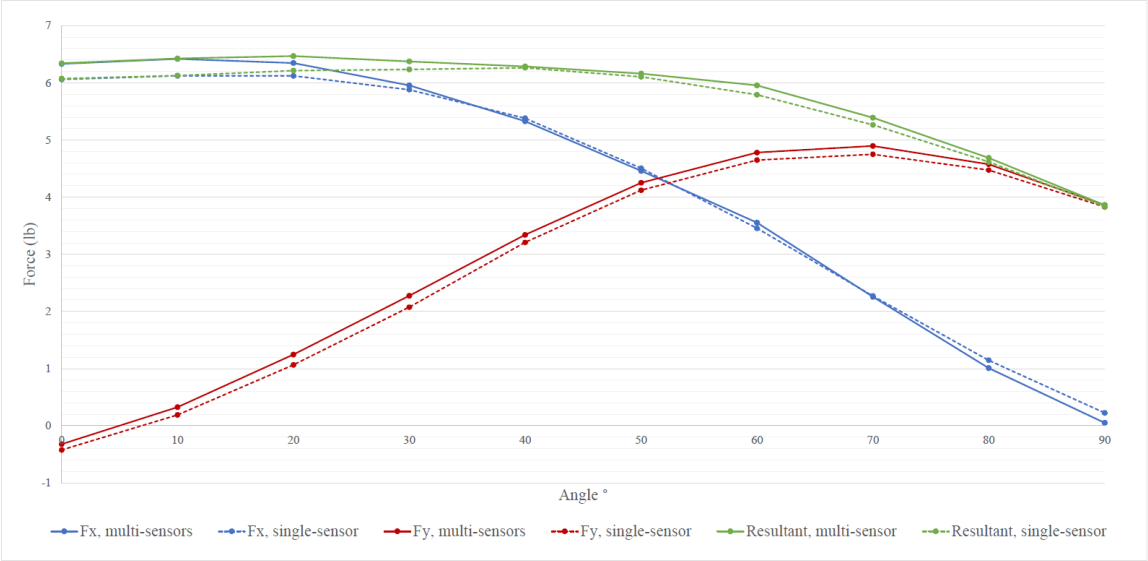

Figure 5.6: Comparison of total base shear measured using single and multiple load cells

A summary result for the base shear on each column of the pre-column detachment model along the X-axis, Y-axis, and resultants is shown in Figures 1, 2, and 3, in Appendix A respectively. It appears that the forces peak at roughly either $\pm 20°$ and $\pm 30°$ along the X-axis and between $\pm 60°$ and $\pm 70°$, similar to what was discussed in Chapter 4.

A summary result for the base shear of the post-column detachment model along the X-axis, Y-axis, and resultants is also shown in Figures 4, 5, and 6, in the Appendix A respectively. The columns in the same column line seem to behave similarly, which is expected considering the shielding effect. Additionally, the interior columns and exterior columns respond slightly differently, which is due to the aerodynamic corner effect in aerodynamic response. A similar trend can be somewhat shown in the results for the pre-column detachment model as well.

The comparison of the total base shear measured in the pre-column detachment model and post-column detachment model is shown in Figure 5.7. This graph shows that there is not any meaningful loss in total base shear between the two tests. In addition, the two models have a similar trend in the overall response.

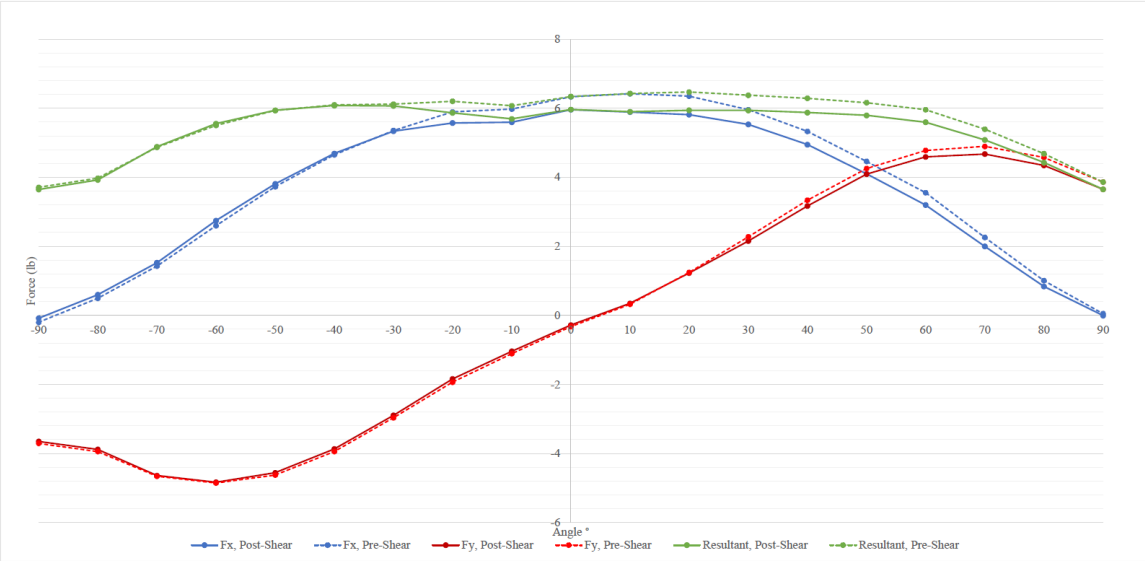

Figure 5.7: A comparison of the total base shear measured in the pre-column detachment and post-column detachment model

It is predicted that the load will be re-distributed to the adjacent columns, namely C2 and D1. The results yield a significant increase for column C1 in addition to C2 and D1, shown in Figures 5.8, 5.9, and 5.10 for the load in X-axis, Y-axis, and resultants, respectively. The percent increase is shown in Figure 5.11. The maximum percent increase occurs at $-30°$ with an increase of about 18 percent. Figures 5.12, 5.13, 5.14, and 5.15 show the increase in the load along X-axis, Y-axis, resultants, and percent increase for column C2, respectively. Similar to Column C1, the peak percent increase happens at $-30°$ with an increase of about 27 percent. On the other hand, Figures 5.16, 5.17, 5.18, and 5.19 show the increase in the load along X-axis, Y-axis, resultants, and percent increase for Column D1, respectively. It seems that the peak percent increase happens at $0°$ as well as $20°$ and $30°$ with an increase of about 35 percent. It appears that the other columns have negligible load increase, as shown in Appendix A.

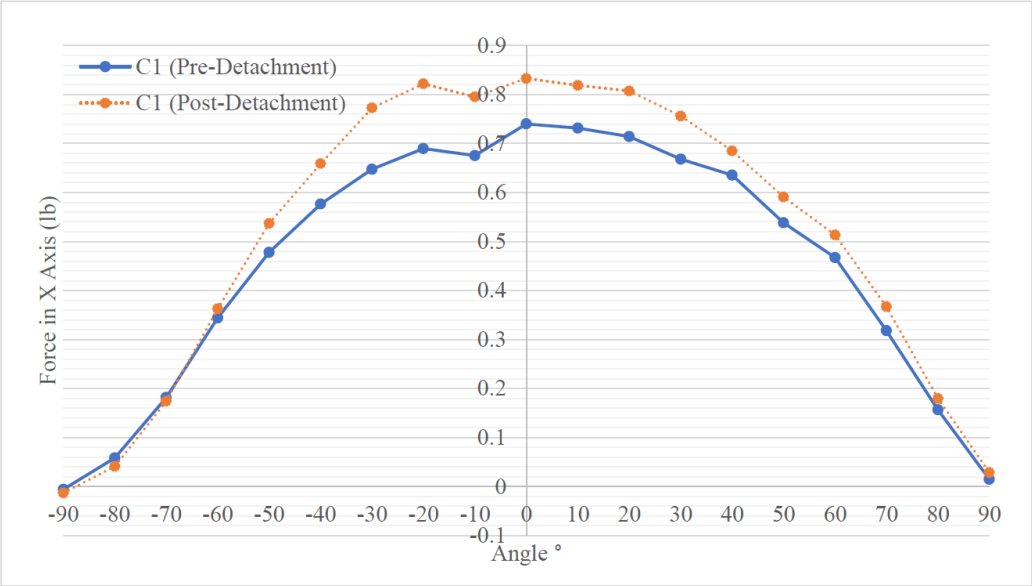

Figure 5.8: Increase in base shear in X-axis for column C1

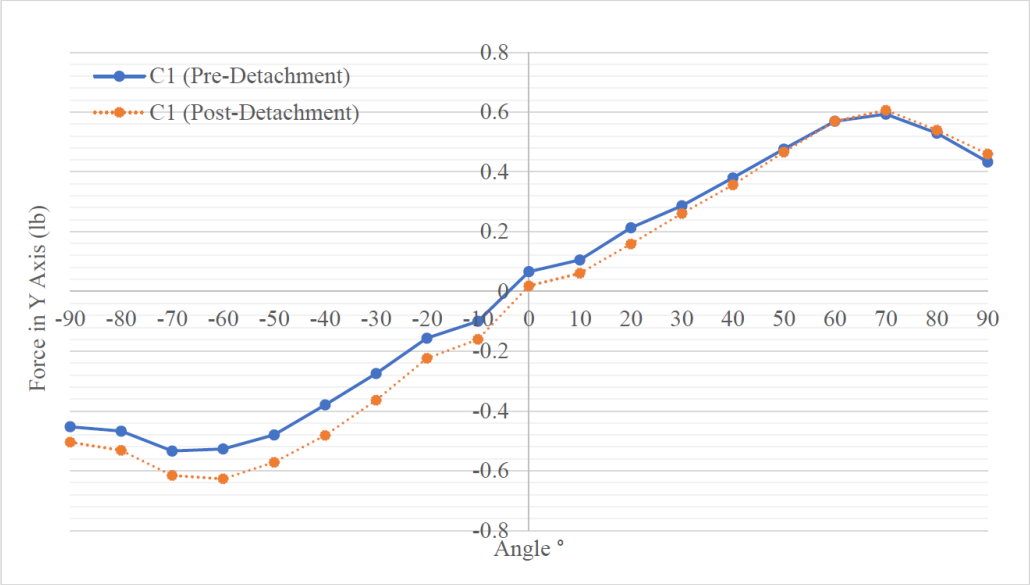

Figure 5.9: Increase in base shear in Y-axis for column C1

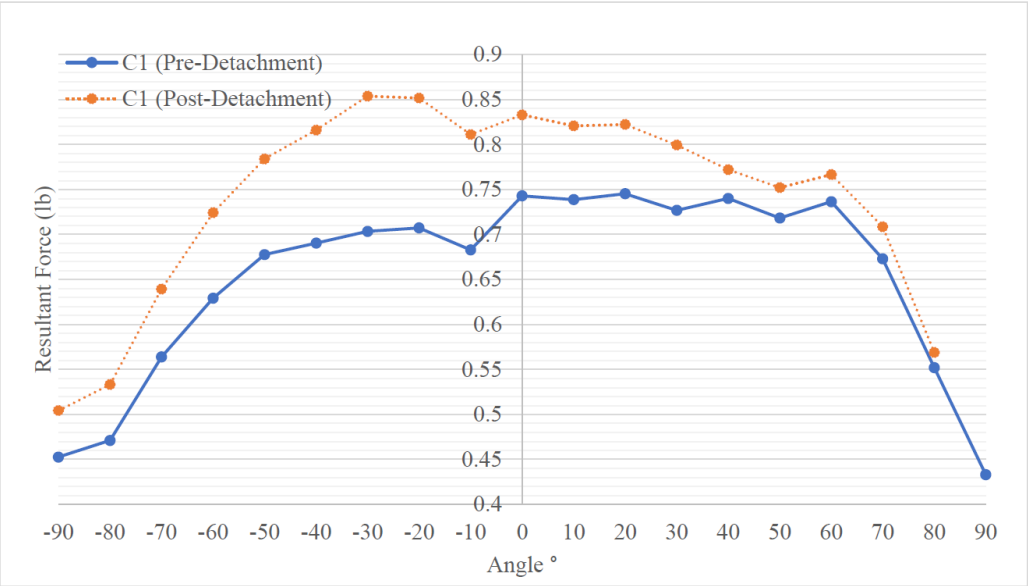

Figure 5.10: Increase in resultant base shear for column C1

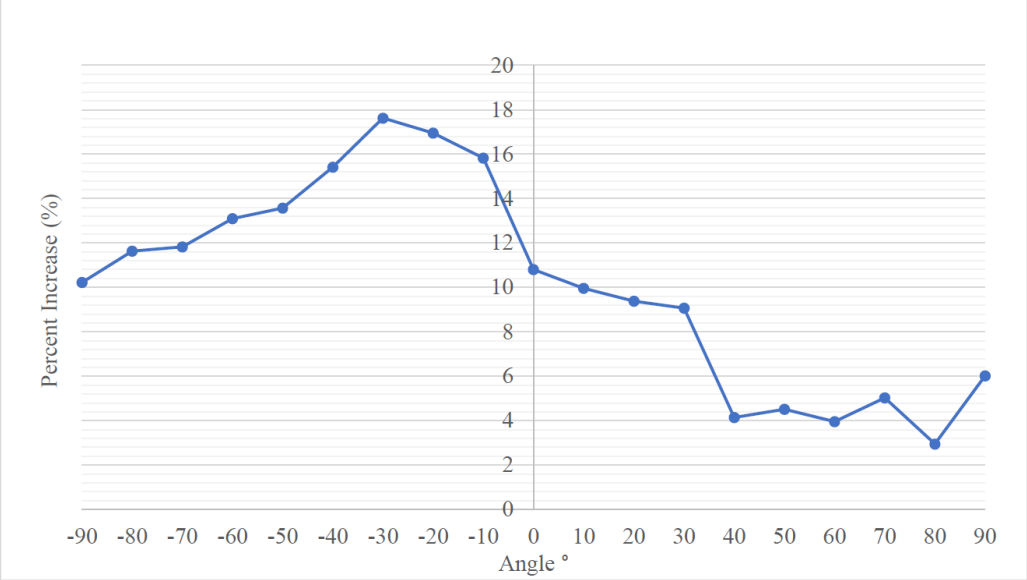

Figure 5.11: Percent increase in resultant base shear for column C1

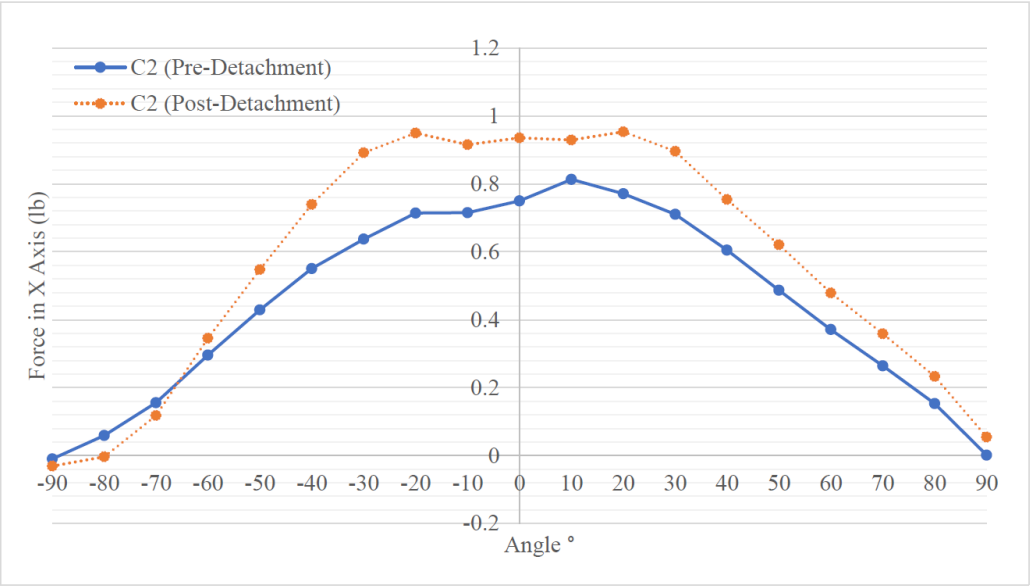

Figure 5.12: Increase in base shear in X-axis for column C2

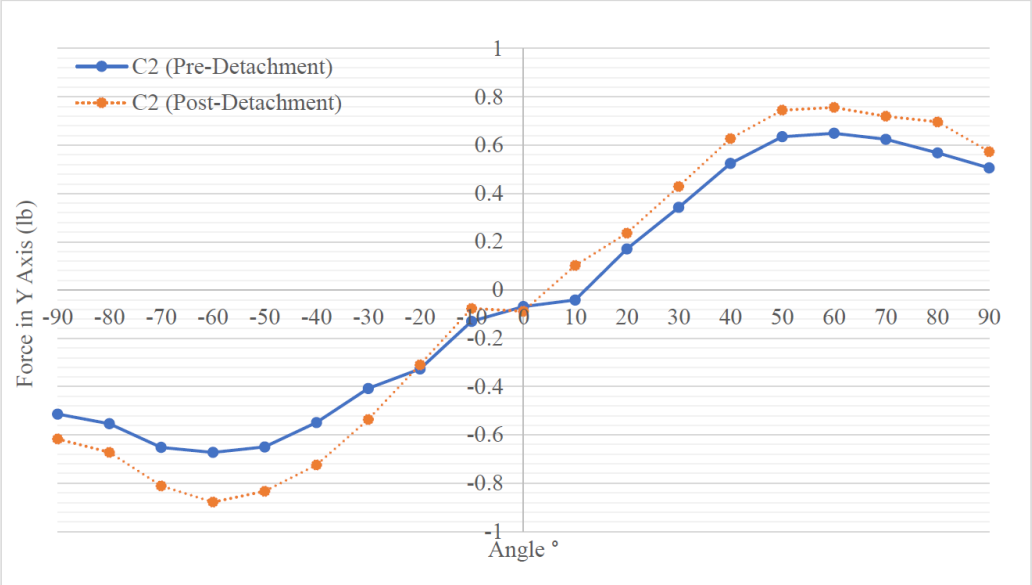

Figure 5.13: Increase in base shear in Y-axis for column C2

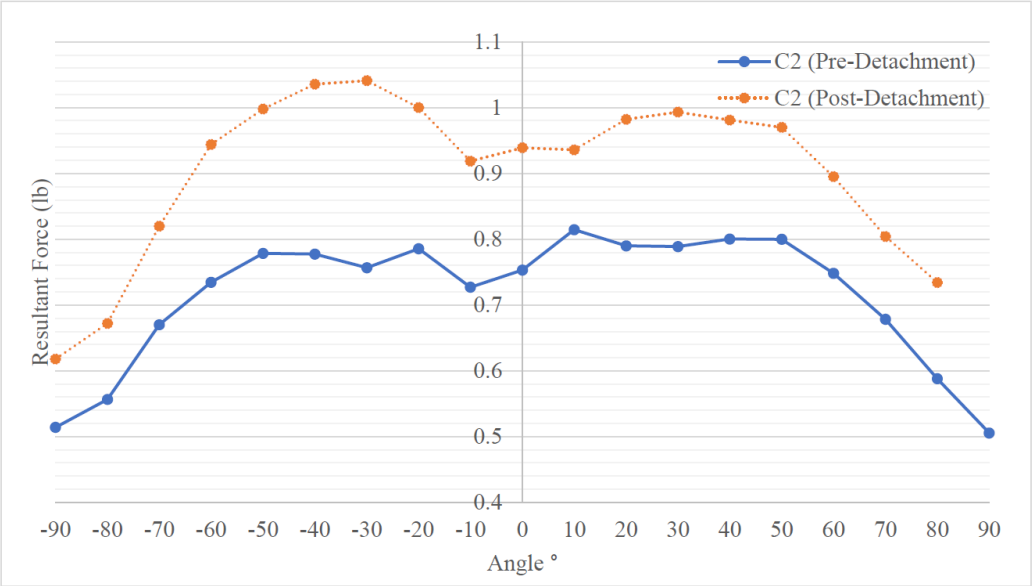

Figure 5.14: Increase in resultant base shear for column C2

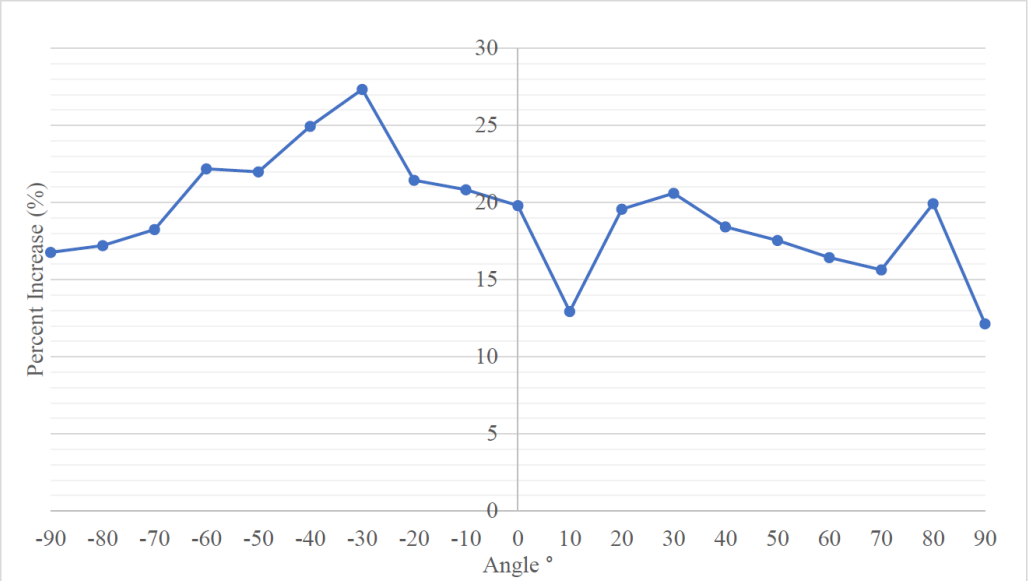

Figure 5.15: Percent increase in resultant base shear for column C2

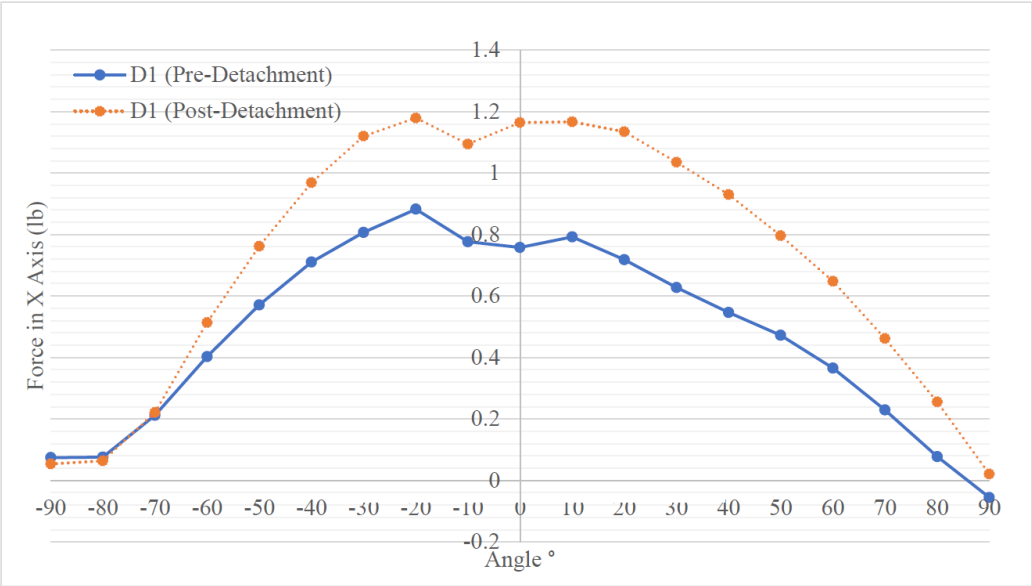

Figure 5.16: Increase in base shear in X-axis for column D1

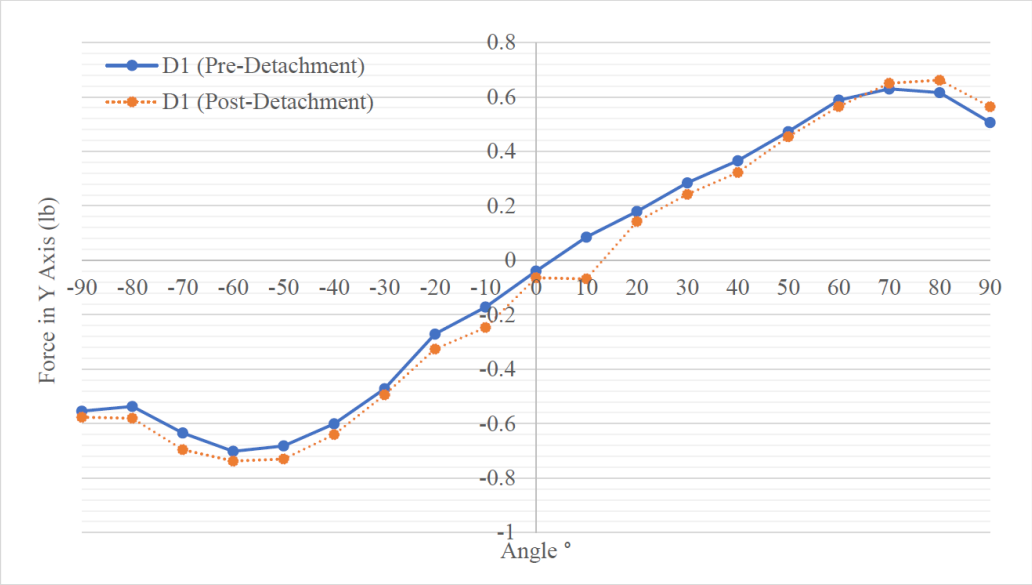

Figure 5.17: Increase in base shear in Y-axis for column D1

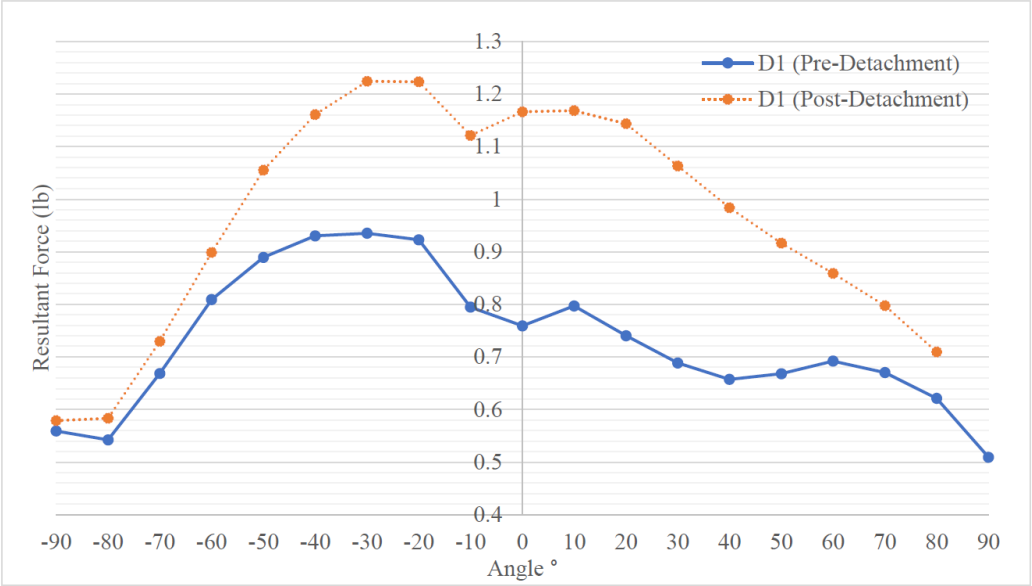

Figure 5.18: Increase in resultant base shear for column D1

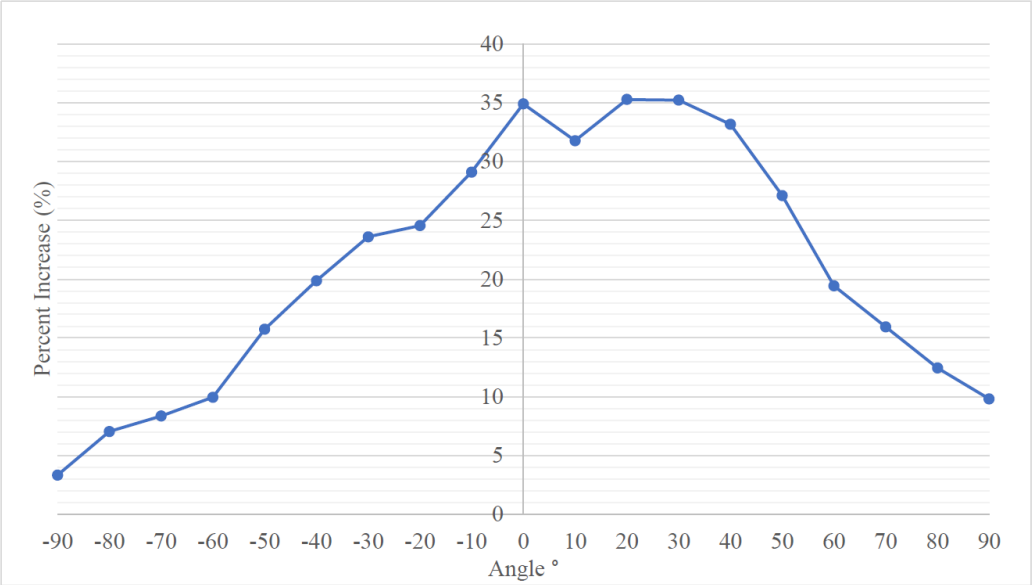

Figure 5.19: Percent increase in resultant base shear for column D1

Chapter 6

Conclusions and Future Work

The force coefficients for single-plane frames provided by AS 1170 and ASCE 7 appear higher than those measured for the wide flange section in this study. A series of force coefficients for wide flange section for flange width to depth ratios of 1.0, 0.9, 0.7, 0.5, and 0.3 is provided in Chapter 3.

A few existing methods for estimating wind loads on pipe racks are reviewed and discussed, and a retrofit strategy is presented. The result shows a 6.3 percent increase in wind load from the intended design (Configuration 1) to the presented retrofit (Configuration 5). Since there is often a need for additional pipelines, additional capacity for future retrofit might be worth considering. The force coefficients for the five configurations of retrofit are provided in Chapter 4. It is shown in Figure 4.6 that the existing design approaches and guidelines discussed in Chapter 2 are sufficient for capturing the increase in wind load induced by the proposed retrofit. It is also observed that the arrangement of pipes might influence the aerodynamic behavior of wind flow and therefore impact the structural response.

The investigation of the influence on wind load during an event, such that a column loses its load-carrying capacity, shows that the overall aerodynamic response of the structure remains similar. The wind load is re-distributed to the adjacent columns and the diagonal one by a considering amount. The result discussed in this study shows that the increase in wind load during an event when a column loses its capacity is not negligible. However, it can be accounted for, providing a proper design method that can be a good study to conduct in the future.

Moving forward, it will be beneficial to investigate a more aerodynamic retrofit strategy

along with its corresponding flow envelope to optimize the structural response. Additionally, there has yet well-documented study for wind-induced load distribution within open-frame structures. Studying the load distribution of such structures would allow a better understanding of the local structural response and provide a better retrofit strategy.

References

[1] ASCE 49. *Wind Tunnel Testing for Buildings and Other Structures*. American Society of Civil Engineers, 2012.

[2] ASCE 67. *ASCE Wind Tunnel Studies of Buildings and Structures, ASCE Manuals and Reports on Engineering Practrice No. 67*. American Society of Civil Engineers, 1999.

[3] ASCE 7. *Minimum Design Loads and Associated Criteria for Buildings and Other Structures*. American Society of Civil Engineers, 2017.

[4] S. D. Amoroso and M. L. Levitan. Recent research for wind loads on petrochemical structures. In *Structures Congress 2009*, pages 1–10, 2009.

[5] E. Calvert and H. Fouad. A review of current wind load provisions for transmission pole structures. *Advanced Technology in Structural Engineering*, pages 1–10, 2000.

[6] Joint Standards Australia/Standards New Zealand Committee et al. Structural design actions—part 2: Wind actions. *AS-NZS*, 1170:2011, 2011.

[7] N. J. Cook. Part 2: Static structures. *The designer's guide to wind loading of building structures*, 1990.

[8] P. N. Georgiou and B. J. Vickery. Wind loads on building frames. In *Wind Engineering*, pages 421–433. Elsevier, 1980.

[9] L. A. Godoy. Performance of storage tanks in oil facilities damaged by hurricanes katrina and rita. *Journal of performance of constructed facilities*, 21(6):441–449, 2007.

[10] IBC. *International Building Code*. International Code Council, 2021.

[11] A. Nadeem and M. Levitan. A refined method for calculating wind load combinations on open-framed structures. *Journal of wind engineering and industrial aerodynamics*, 72:445–453, 1997.

[12] Task Committee on Wind-Induced Forces and ASCE Task Committee on Anchor Bolt Design of the Petrochemical Committee of the Energy Division. Wind loads and anchor bolt design for petrochemical facilities. American Society of Civil Engineers, 1997.

[13] S. Ou, W. Pang, and M. Stoner. Drag coefficients and wind loads of retrofitted pipe racks with high blockage ratios. In *Proceedings of 6th AAWE Workshop*, 2021.

[14] L. Qiang. *Wind tunnel tests for wind loads on open frame petrochemical structures*. PhD thesis, Louisiana State University, Baton Rouge, 1998.

[15] ASCE Task Committee on Wind-Induced Forces of the Petrochemical Committee of Energy Division. Wind loads for petrochemical and other industrial facilities. American Society of Civil Engineers, 2011.

[16] M. R. Willford and A. C. Allsop. *Design guide for wind loads on unclad framed building structures during construction: supplement 3 to The designer's guide to wind loading of building structures*. Building Research Establishment, 1990.

Appendices

Appendix A Detailed Load Re-Distribution Test Results

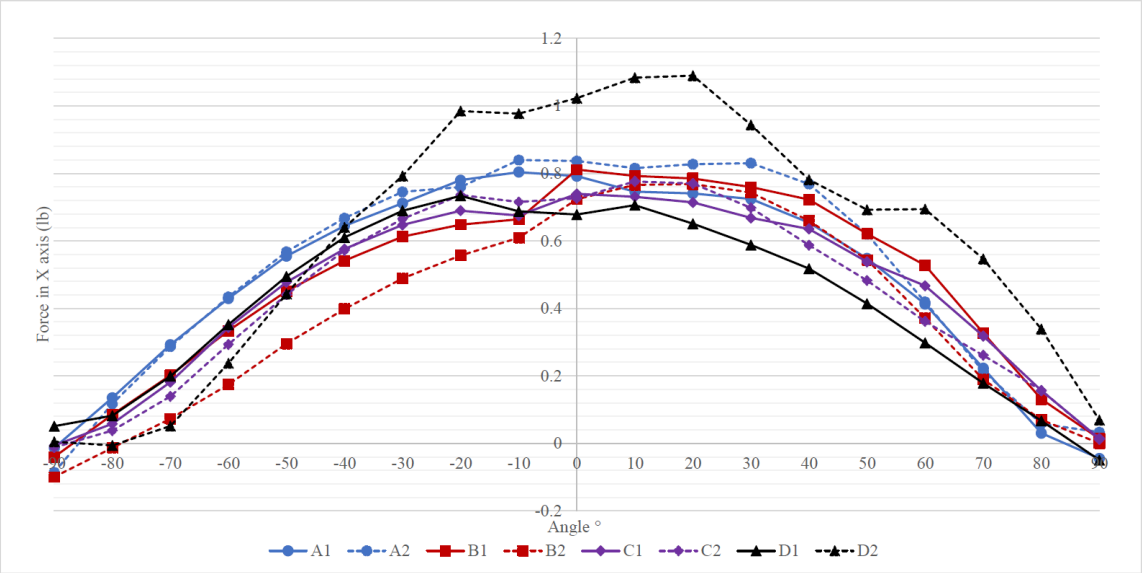

Figure 1: A summary result for base shear in X-axis for the pre-column detachment model

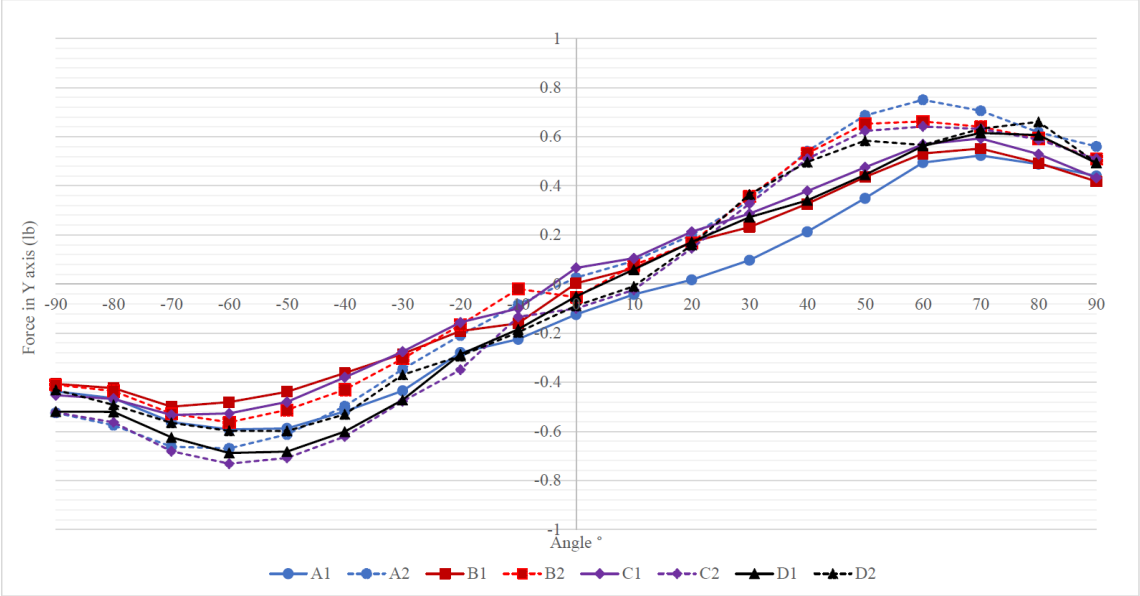

Figure 2: A summary result for base shear in Y-axis for the pre-column detachment model

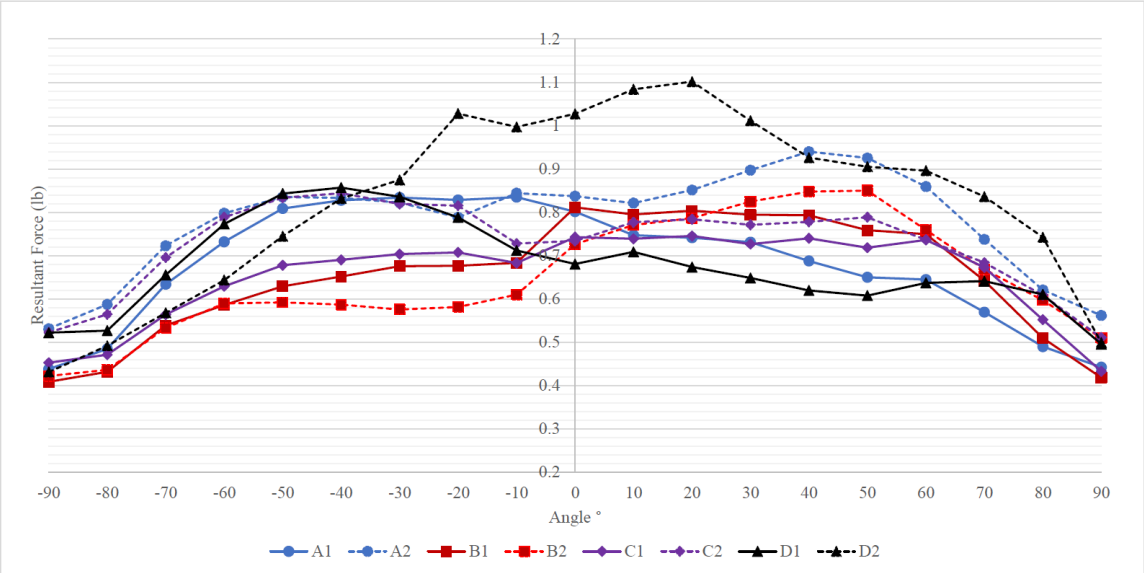

Figure 3: A summary result for resultant base shear for the pre-column detachment model

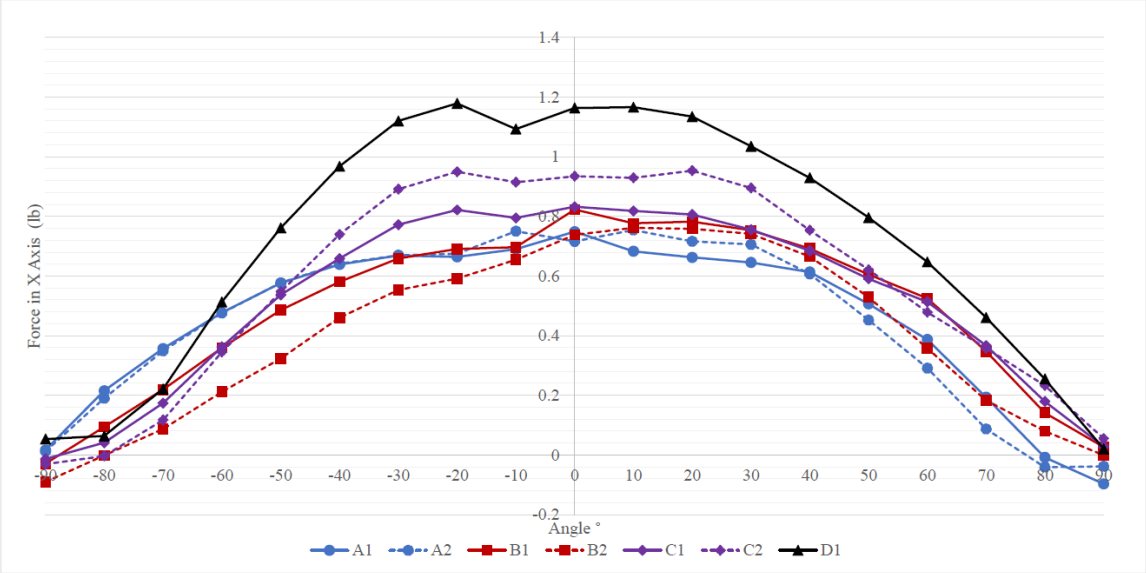

Figure 4: A summary result for base shear in X-axis for the post-column detachment model

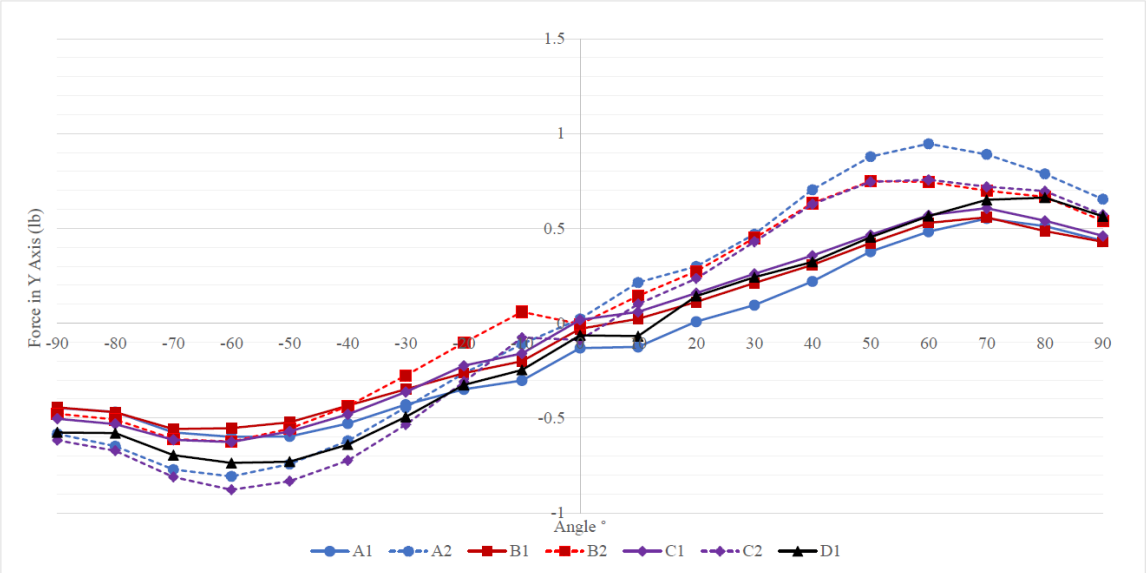

Figure 5: A summary result for base shear in Y-axis for the post-column detachment model

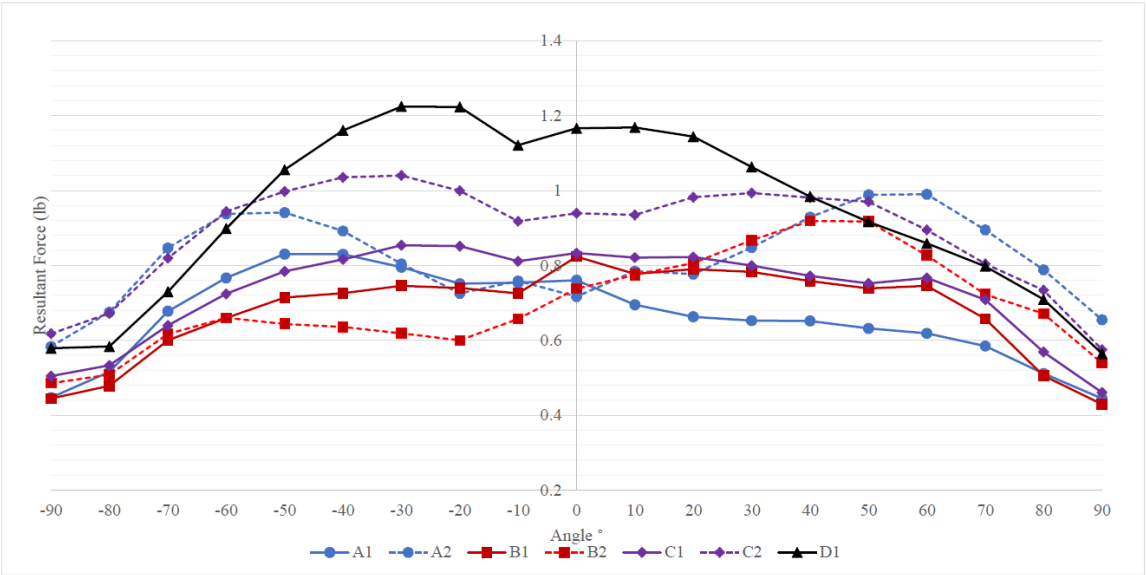

Figure 6: A summary result for resultant base shear for the post-column detachment model

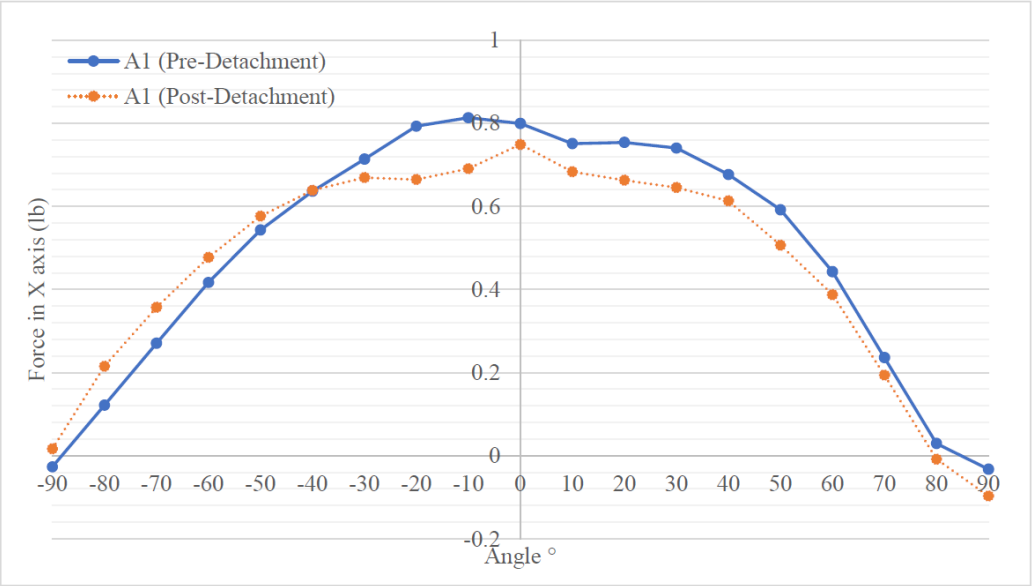

Figure 7: Increase in base shear in X-axis for column A1

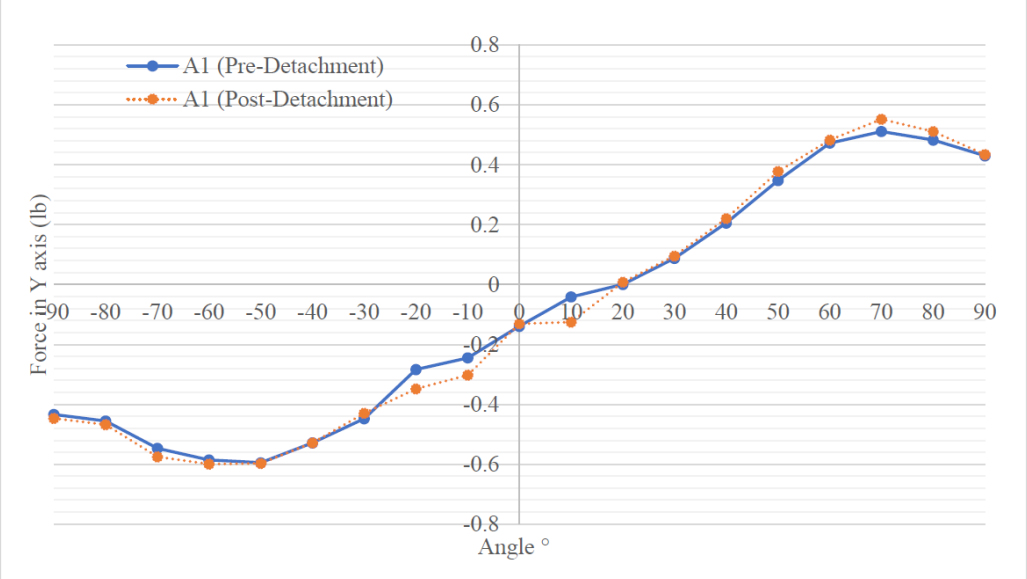

Figure 8: Increase in base shear in Y-axis for column A1

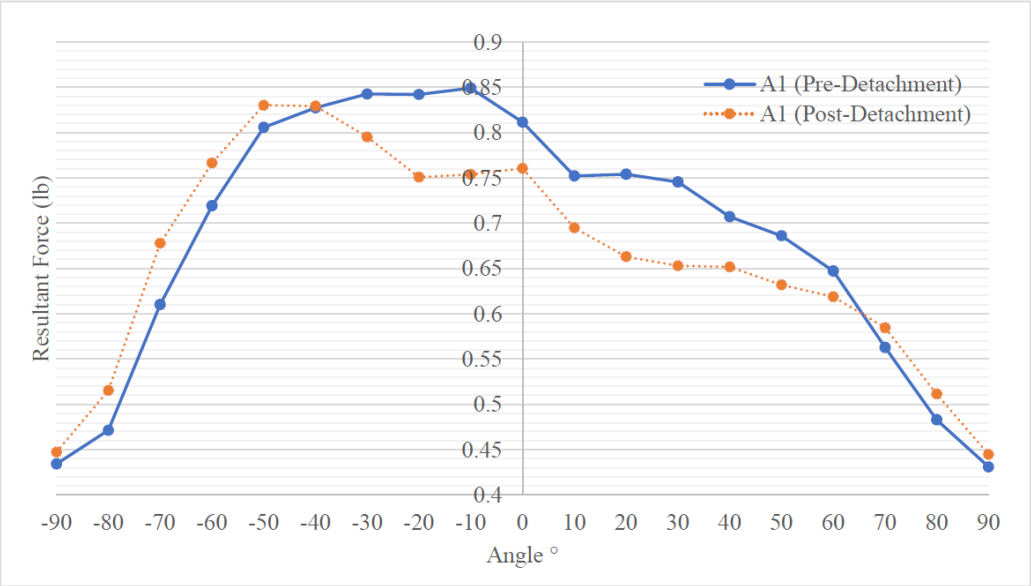

Figure 9: Increase in resultant base shear for column A1

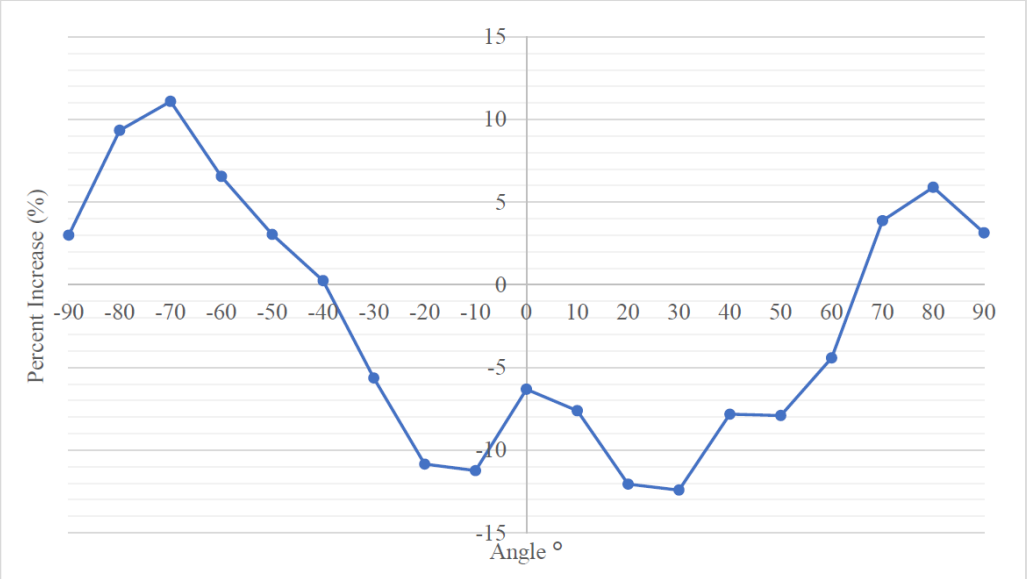

Figure 10: Percent increase in resultant base shear for column A1

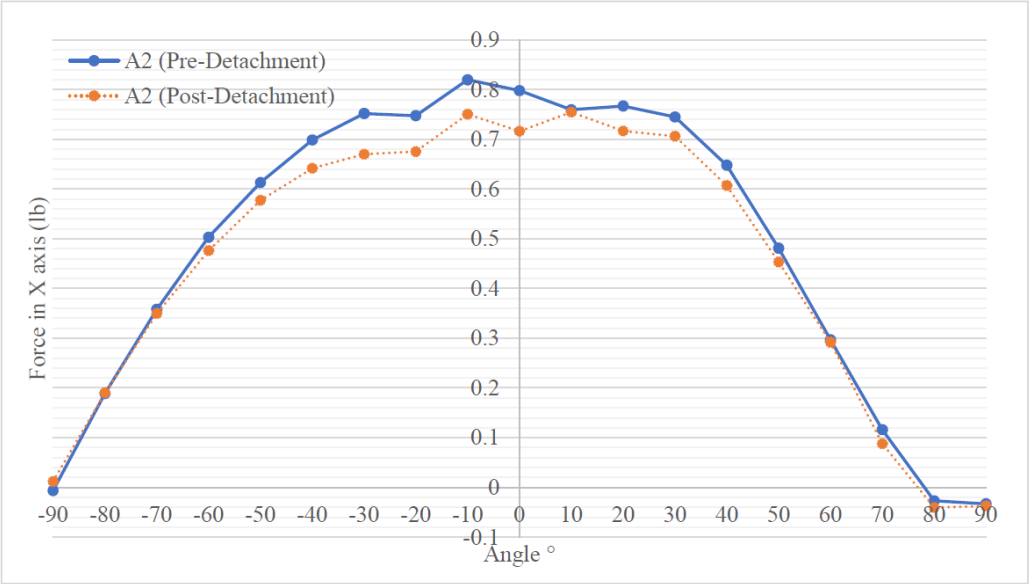

Figure 11: Increase in base shear in X-axis for column A2

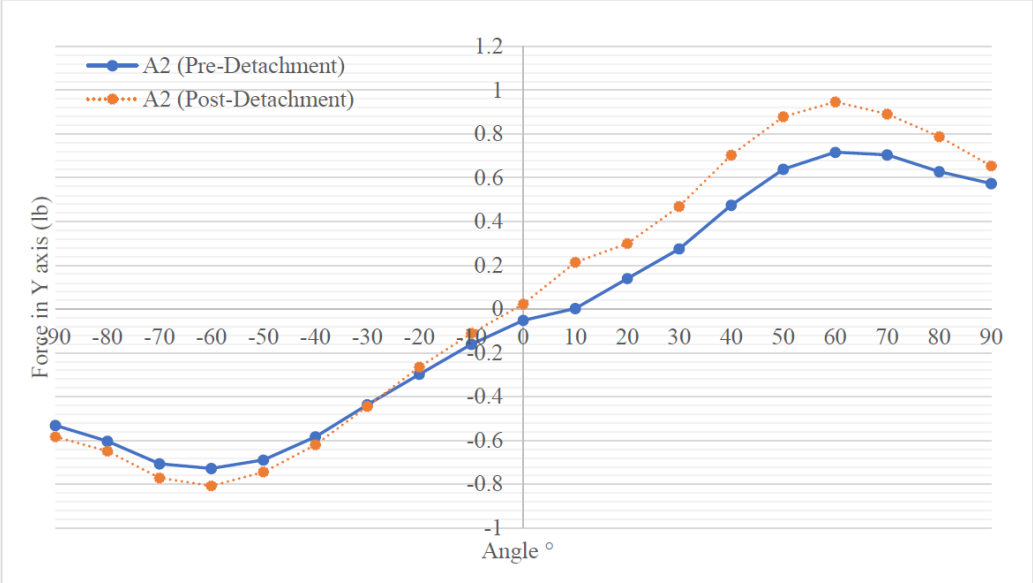

Figure 12: Increase in base shear in Y-axis for column A2

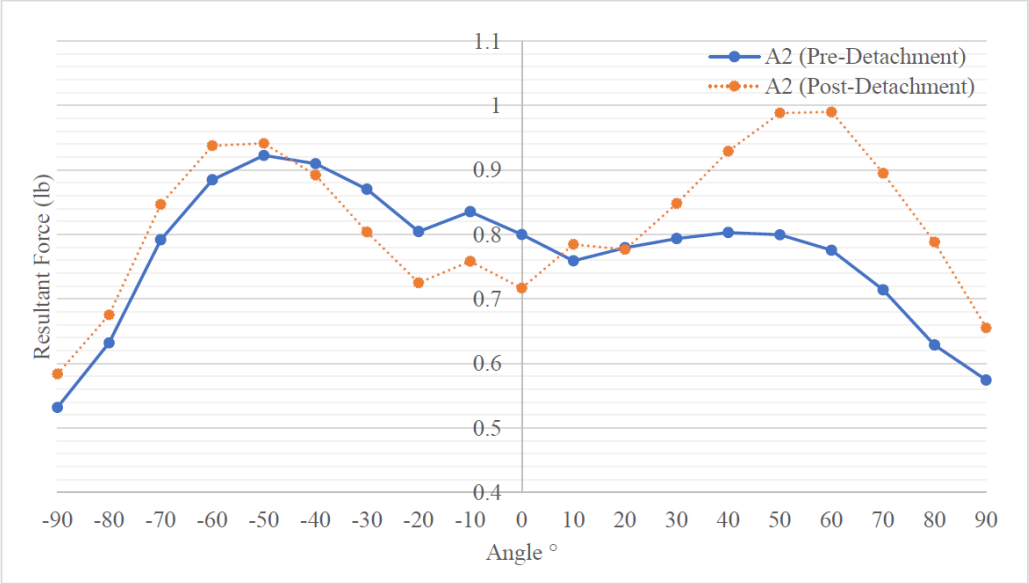

Figure 13: Increase in resultant base shear for column A2

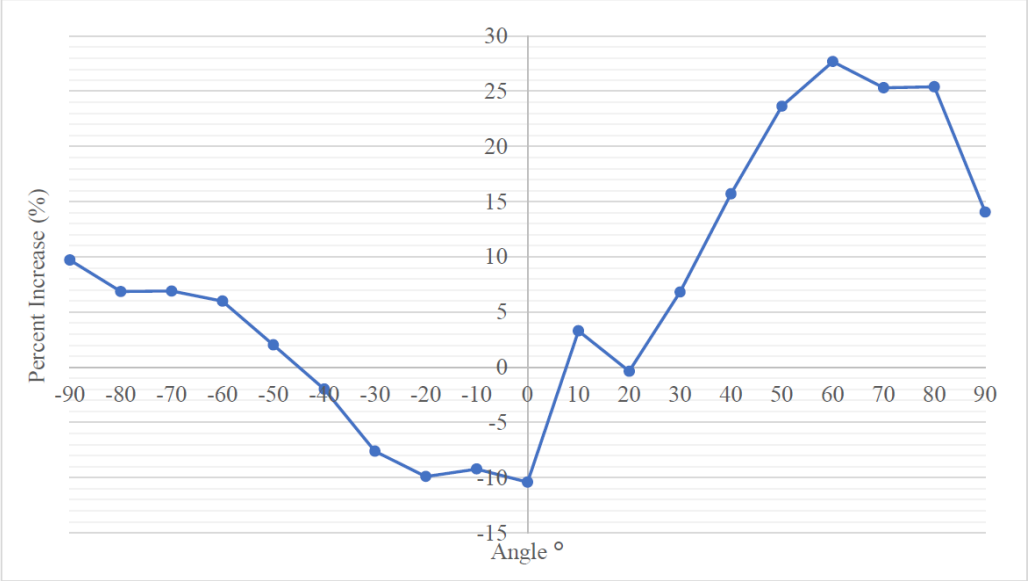

Figure 14: Percent increase in resultant base shear for column A2

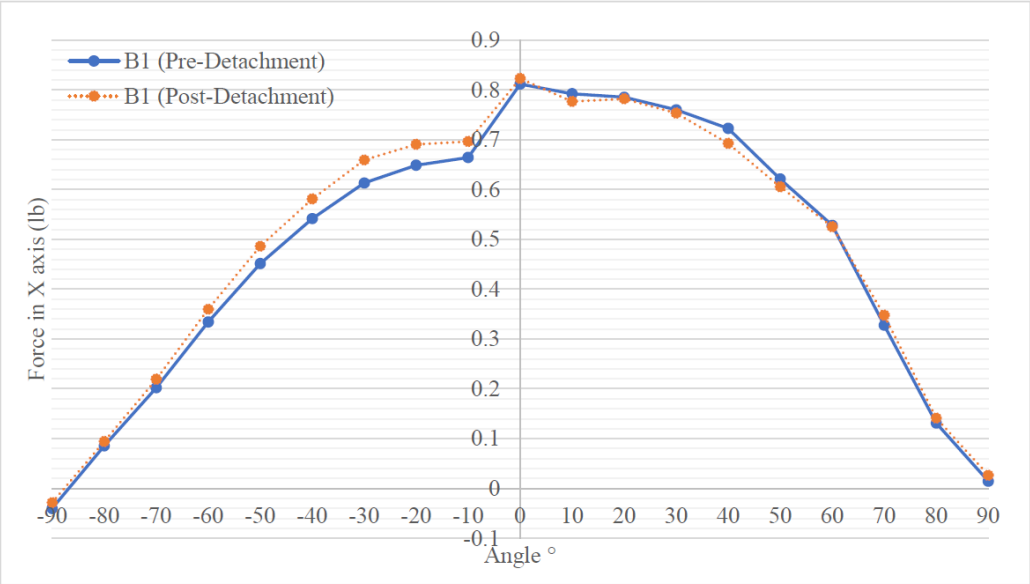

Figure 15: Increase in base shear in X-axis for column B1

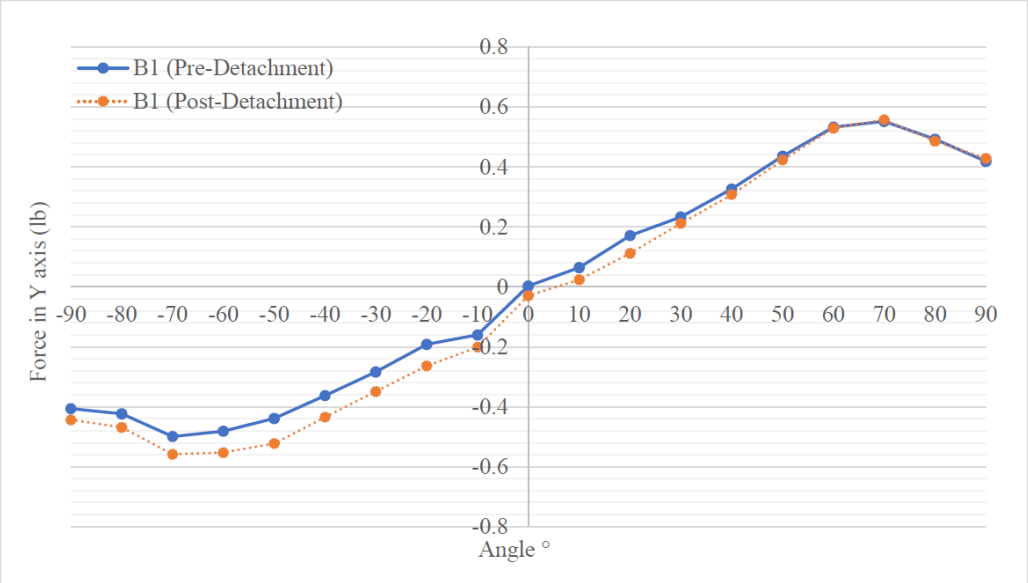

Figure 16: Increase in base shear in Y-axis for column B1

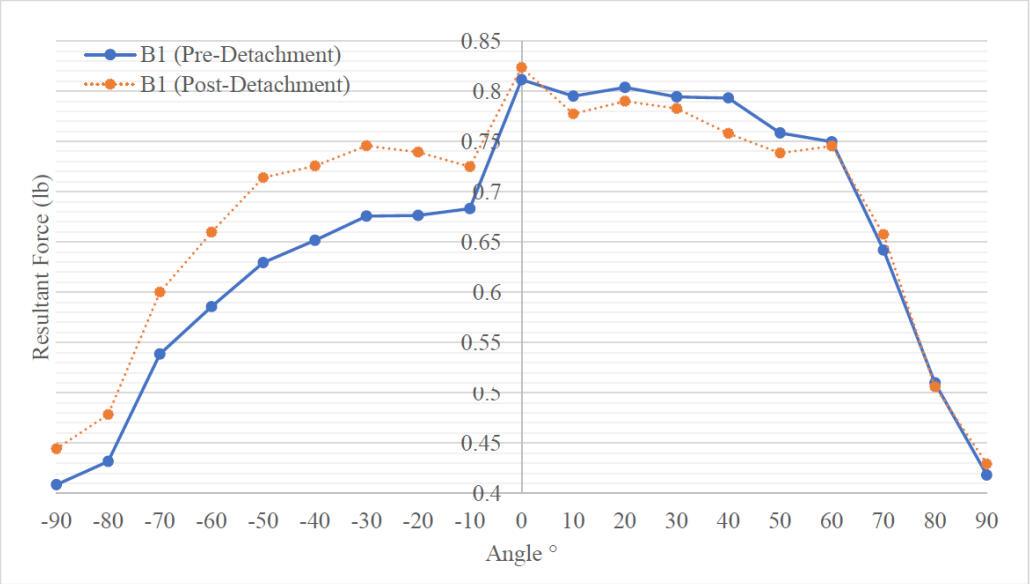

Figure 17: Increase in resultant base shear for column B1

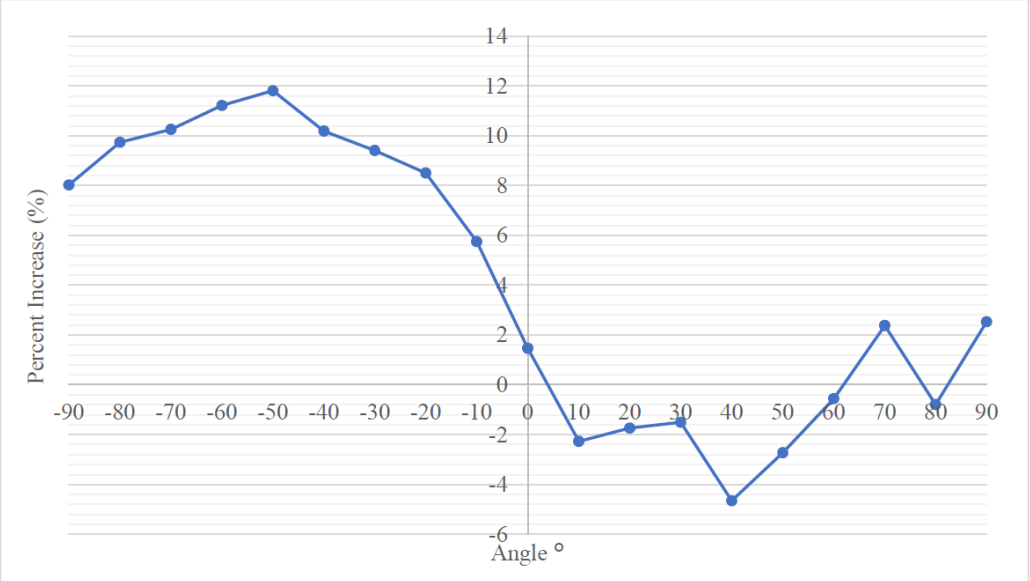

Figure 18: Percent increase in resultant base shear for column B1

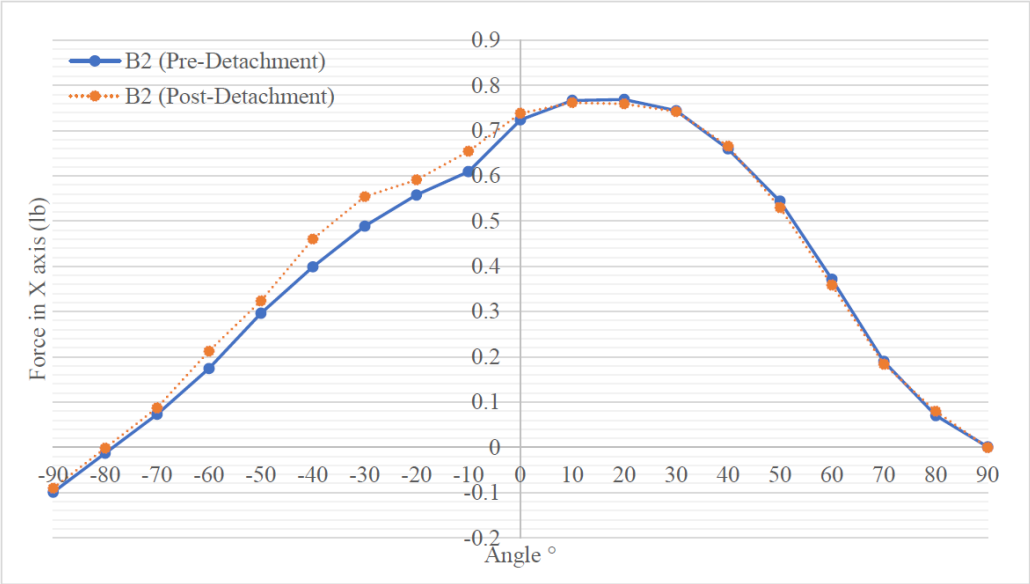

Figure 19: Increase in base shear in X-axis for column B2

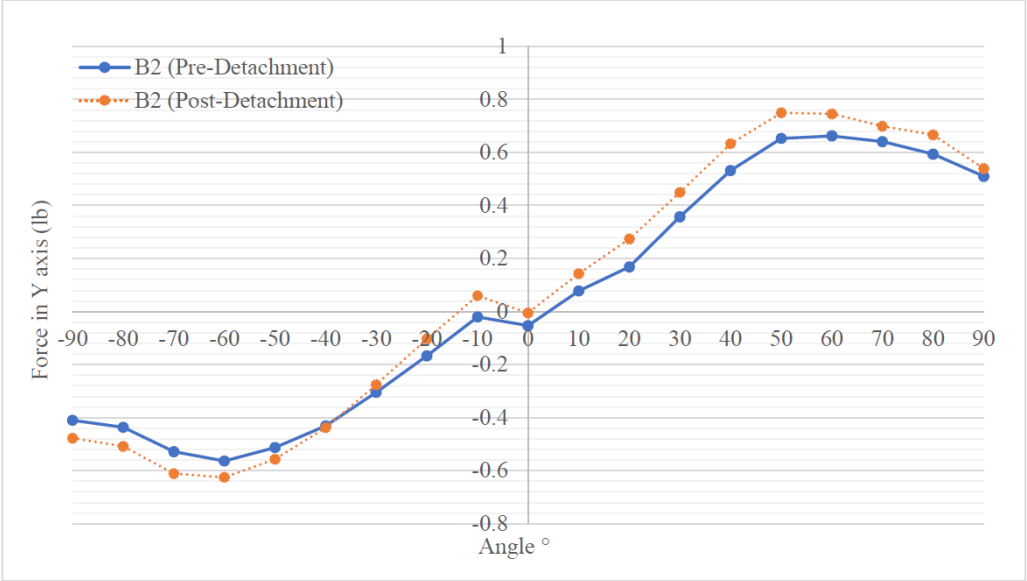

Figure 20: Increase in base shear in Y-axis for column B2

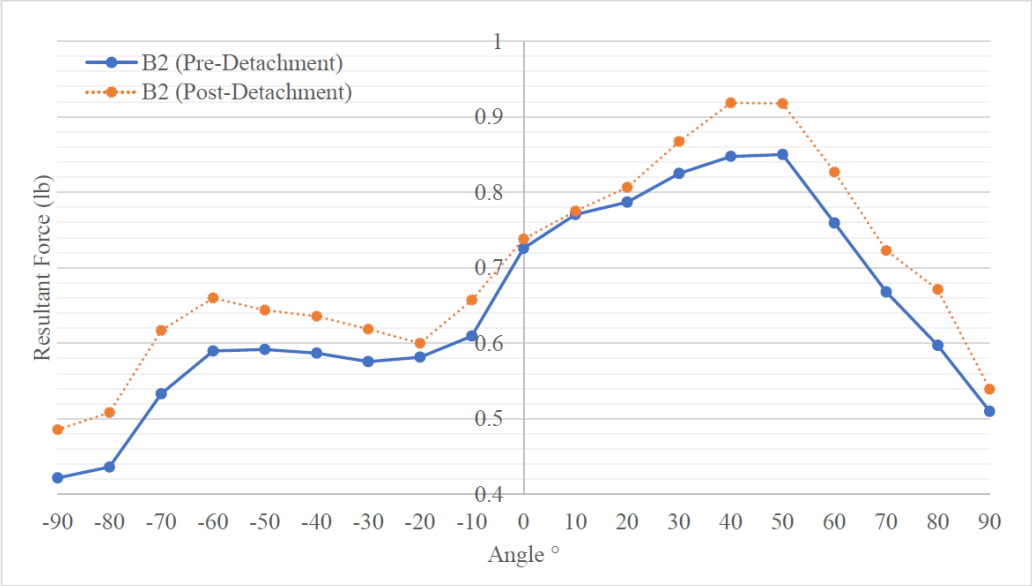

Figure 21: Increase in resultant base shear for column B2

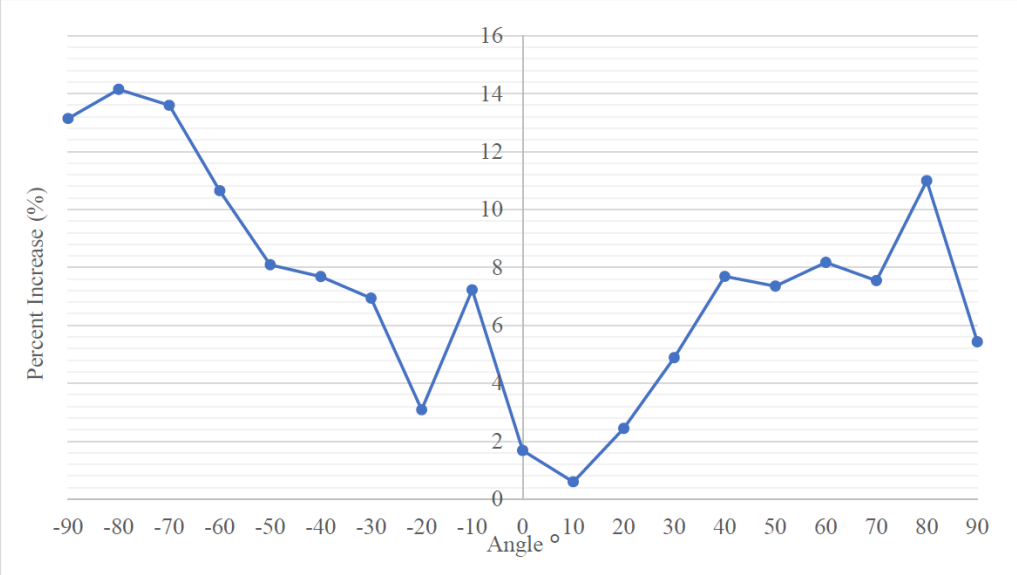

Figure 22: Percent increase in resultant base shear for column B2

Appendix B Estimation of Wind Load for Pipe Rack Model

Appendix B Estimation of Wind Load for Pipe Rack Model

WIND LOAD:

$V := 31$ mph $G := 1$

$q := 0.00256 \cdot V^2 \cdot psf = 2.46\ psf$

SECTION 5.1:

Stage 1:

Pipes: $d_{max} := \frac{3}{15}\ ft$ $C_{f\_pipe} := 0.7$ $L := \frac{30}{15}\ ft$

$A_{e\_pipe} := d_{max} + 0.1 \cdot \frac{10}{15}\ ft = 0.267\ \frac{ft^2}{ft}$

$F_{pipe} := 2 \cdot q \cdot G \cdot C_{f\_pipe} \cdot A_{e\_pipe} \cdot L = 1.837\ lbf$

Structural members: $C_{f\_s} := 1.8$ Sec.5.1.3

$h := \frac{20}{15}\ ft$ $d := 0.98\ in$ $b_f := 0.98\ in$

$A_{e\_stringers} := 3 \cdot d \cdot L = 0.49\ ft^2$

$A_{e\_columns} := 4 \cdot b_f \cdot h = 0.436\ ft^2$

$F_s := q \cdot G \cdot C_{f\_s} \cdot \langle A_{e\_stringers} + A_{e\_columns} + 4 \cdot 3.62\ in \cdot 0.25\ in \rangle = 4.21\ lbf$

$F := F_{pipe} + F_s = 6.047\ lbf$

Stage 2:

Pipes: $d_1 := \frac{1}{15}\ ft$ $C_{f\_pipe} := 0.7$ $L := \frac{30}{15}\ ft$ $d_2 := \frac{3}{15}\ ft$

$A_{e\_pipe1} := d_1 + 0.1 \cdot \frac{10}{15}\ ft = 0.133\ \frac{ft^2}{ft}$

$F_{pipe1} := q \cdot G \cdot C_{f\_pipe} \cdot A_{e\_pipe1} \cdot L = 0.459\ lbf$

$A_{e\_pipe2} := d_2 + 0.1 \cdot \frac{10}{15}\ ft = 0.267\ \frac{ft^2}{ft}$

$F_{pipe2} := 2 \cdot q \cdot G \cdot C_{f\_pipe} \cdot A_{e\_pipe2} \cdot L = 1.837\ lbf$

$F_{pipe} := F_{pipe1} + F_{pipe2} = 2.296\ lbf$

Structural members: $C_{f\_s} := 1.8$ Sec.5.1.3

$A_{e\_stringers} := 3 \cdot d \cdot L = 0.49\ ft^2$

$A_{e\_columns} := 4 \cdot b_f \cdot h = 0.436\ ft^2$

$F_s := q \cdot G \cdot C_{f\_s} \cdot \langle A_{e\_stringers} + A_{e\_columns} + 4 \cdot 3.62\ in \cdot 0.25\ in \rangle = 4.21\ lbf$

$F := F_{pipe} + F_s = 6.506\ lbf$

Stage 3:

Pipes: $d_1 := \frac{1}{15}\ ft$ $C_{f\_pipe} := 0.7$ $L := \frac{30}{15}\ ft$ $d_2 := \frac{3}{15}\ ft$

$A_{e\_pipe1} := d_1 + 0.1 \cdot \frac{10}{15}\ ft = 0.133\ \frac{ft^2}{ft}$

$F_{pipe1} := q \cdot G \cdot C_{f\_pipe} \cdot A_{e\_pipe1} \cdot L = 0.459\ lbf$

$A_{e\_pipe2} := d_2 + 0.1 \cdot \frac{10}{15}\ ft = 0.267\ \frac{ft^2}{ft}$

$F_{pipe2} := q \cdot G \cdot C_{f\_pipe} \cdot A_{e\_pipe2} \cdot L = 0.918\ lbf$

$A_{e\_pipe3} := d_2 + 0.1 \cdot \frac{20}{15}\ ft = 0.333\ \frac{ft^2}{ft}$

$F_{pipe3} := q \cdot G \cdot C_{f\_pipe} \cdot A_{e\_pipe3} \cdot L = 1.148\ lbf$

$F_{pipe} := F_{pipe1} + F_{pipe2} + F_{pipe3} = 2.526\ lbf$

Structural members: $C_{f\_s} := 1.8$ Sec.5.1.3

$h := \frac{20}{15}\ ft$

$A_{e\_stringers} := 3 \cdot d \cdot L = 0.49\ ft^2$

$A_{e\_columns} := 4 \cdot b_f \cdot h = 0.436\ ft^2$

$F_s := q \cdot G \cdot C_{f\_s} \cdot \langle A_{e\_stringers} + A_{e\_columns} + 4 \cdot 3.62\ in \cdot 0.25\ in \rangle = 4.21\ lbf$

$F := F_{pipe} + F_s = 6.736\ lbf$

Stage 4:

Pipes: $d_1 := \frac{1}{15}\ ft$ $C_{f\_pipe} := 0.7$ $L := \frac{30}{15}\ ft$ $d_2 := \frac{3}{15}\ ft$

$A_{e\_pipe1} := d_1 + 0.1 \cdot \frac{10}{15}\ ft = 0.133\ \frac{ft^2}{ft}$

$F_{pipe1} := q \cdot G \cdot C_{f\_pipe} \cdot A_{e\_pipe1} \cdot L = 0.459\ lbf$

$A_{e\_pipe2} := d_2 + 0.1 \cdot \frac{20}{15}\ ft = 0.333\ \frac{ft^2}{ft}$

$F_{pipe2} := q \cdot G \cdot C_{f\_pipe} \cdot A_{e\_pipe2} \cdot L = 1.148\ lbf$

$A_{e\_pipe3} := d_2 + 0.1 \cdot \frac{20}{15}\ ft = 0.333\ \frac{ft^2}{ft}$

$F_{pipe3} := q \cdot G \cdot C_{f\_pipe} \cdot A_{e\_pipe3} \cdot L = 1.148\ lbf$

$F_{pipe} := F_{pipe1} + F_{pipe2} + F_{pipe3} = 2.755\ lbf$

Structural members: $C_{f\_s} := 1.8$ Sec.5.1.3

$h := \frac{20}{15}\ ft$

$A_{e\_stringers} := 3 \cdot d \cdot L = 0.49\ ft^2$

$A_{e\_columns} := 4 \cdot b_f \cdot h = 0.436\ ft^2$

$F_s := q \cdot G \cdot C_{f\_s} \cdot \langle A_{e\_stringers} + A_{e\_columns} + 4 \cdot 3.62\ in \cdot 0.25\ in \rangle = 4.21\ lbf$

$F := F_{pipe} + F_s = 6.965\ lbf$

Stage 5:

Pipes: $d_1 := \frac{1}{15}\ ft$ $C_{f\_pipe} := 0.7$ $L := \frac{30}{15}\ ft$ $d_2 := \frac{3}{15}\ ft$

$A_{e\_pipe1} := d_1 + 0.1 \cdot \frac{20}{15}\ ft = 0.2\ \frac{ft^2}{ft}$

$F_{pipe1} := q \cdot G \cdot C_{f\_pipe} \cdot A_{e\_pipe1} \cdot L = 0.689\ lbf$

$A_{e\_pipe2} := d_2 + 0.1 \cdot \frac{20}{15}\ ft = 0.333\ \frac{ft^2}{ft}$

$F_{pipe2} := q \cdot G \cdot C_{f\_pipe} \cdot A_{e\_pipe2} \cdot L = 1.148\ lbf$

$A_{e\_pipe3} := d_2 + 0.1 \cdot \frac{20}{15}\ ft = 0.333\ \frac{ft^2}{ft}$

$F_{pipe3} := q \cdot G \cdot C_{f\_pipe} \cdot A_{e\_pipe3} \cdot L = 1.148\ lbf$

$F_{pipe} := F_{pipe1} + F_{pipe2} + F_{pipe3} = 2.985\ lbf$

Structural members: $C_{f\_s} := 1.8$ Sec.5.1.3

$h := \frac{20}{15}\ ft$

$A_{e\_stringers} := 3 \cdot d \cdot L = 0.49\ ft^2$

$A_{e\_columns} := 4 \cdot b_f \cdot h = 0.436\ ft^2$

$F_s := q \cdot G \cdot C_{f\_s} \cdot \left\langle A_{e\_stringers} + A_{e\_columns} + 4 \cdot 3.62\ in \cdot 0.25\ in \right\rangle = 4.21\ lbf$

$F := F_{pipe} + F_s = 7.195\ lbf$

$M := F \cdot 12\ in + F \cdot 8\ in = 143.899\ lbf \cdot in$

APPENDIX 5B:

Stage 1:

$L := \frac{10}{15}\ ft \qquad B := \frac{30}{15}\ ft \qquad H := \frac{20}{15}\ ft$

$A_g := B \cdot H = 2.667\ ft^2$

$\frac{L}{B} = 0.333$

$C_{f1} := \frac{1}{4} \cdot \left(\frac{L}{B}\right)^2 + 1.4 = 1.428$

$F := q \cdot G \cdot C_{f1} \cdot A_g = 9.367\ lbf$

Stage 2:

$L := \frac{10}{15}\ ft \qquad B := \frac{30}{15}\ ft \qquad H := \frac{21}{15}\ ft$

$A_g := B \cdot H = 2.8\ ft^2$

$\frac{L}{B} = 0.333$

$C_{f1} := \frac{1}{4} \cdot \left(\frac{L}{B}\right)^2 + 1.4 = 1.428$

$F := q \cdot G \cdot C_{f1} \cdot A_g = 9.835\ lbf$

Stage 3:

$L := \frac{20}{15}\ ft \qquad B := \frac{30}{15}\ ft \qquad H := \frac{21}{15}\ ft$

$A_{g2} := \frac{7.5}{15}\ ft \cdot B = 1\ ft^2$

$A_{g1} := \frac{13.5}{15}\ ft \cdot B = 1.8\ ft^2$

$\frac{L}{B} = 0.667$

$C_{f2} := \frac{1}{4} \cdot \left(\frac{L}{B}\right)^2 + 1.4 = 1.511$

$F := q \cdot G \cdot \left(C_{f1} \cdot A_{g1} + C_{f2} \cdot A_{g2}\right) = 10.04\ lbf$

Stage 4:

$L := \frac{20}{15}\ ft \qquad B := \frac{30}{15}\ ft \qquad H := \frac{21}{15}\ ft$

$A_{g2} := \frac{12.5}{15}\ ft \cdot B = 1.667\ ft^2$

$A_{g1} := \frac{8.5}{15}\ ft \cdot B = 1.133\ ft^2$

$\frac{L}{B} = 0.667$

$C_{f2} := \frac{1}{4} \cdot \left(\frac{L}{B}\right)^2 + 1.4 = 1.511$

$F := q \cdot G \cdot \left(C_{f1} \cdot A_{g1} + C_{f2} \cdot A_{g2}\right) = 10.177\ lbf$

Stage 5:

$L := \frac{20}{15}\ ft \qquad B := \frac{30}{15}\ ft \qquad H := \frac{21}{15}\ ft$

$A_{g2} := H \cdot B = 2.8\ ft^2$

$\frac{L}{B} = 0.667$

$C_{f2} := \frac{1}{4} \cdot \left(\frac{L}{B}\right)^2 + 1.4 = 1.511$

$F := q \cdot G \cdot C_{f2} \cdot A_{g2} = 10.409\ lbf$

$M := F \cdot 12\ in + F \cdot 8\ in = 208.184\ lbf \cdot in$

SECTION 5.1-Alternative 2:

Stage 1:

Pipes: $d_{max} := \frac{3}{15}\ ft \quad C_{f\_pipe} := 0.7 \quad L := \frac{30}{15}\ ft$

$A_{e\_pipe} := d_{max} + 0.1 \cdot \frac{10}{15}\ ft = 0.267\ \frac{ft^2}{ft}$

$F_{pipe} := 2 \cdot q \cdot G \cdot C_{f\_pipe} \cdot A_{e\_pipe} \cdot L = 0.002\ kip$

Structural members:

First Level: $C_{f\_s} := 2.0 \quad h := \frac{12.5}{15}\ ft$

$A_{e\_stringers} := 1 \cdot d \cdot L = 0.163\ ft^2$

$A_{e\_columns} := 4 \cdot b_f \cdot h = 0.272\ ft^2$

$F_{s1} := q \cdot G \cdot C_{f\_s} \cdot \left(A_{e\_stringers} + A_{e\_columns} + 4 \cdot 3.62\ in \cdot 0.25\ in\right) = 2.267\ lbf$

Higher Level: $C_{f\_s} := 1.6 \quad h := \frac{7.5}{15}\ ft$

$A_{e\_stringers} := 2 \cdot d \cdot L = 0.327\ ft^2$

$A_{e\_columns} := 4 \cdot b_f \cdot h = 0.163\ ft^2$

$F_{s2} := q \cdot G \cdot C_{f\_s} \cdot \left(A_{e\_stringers} + A_{e\_columns}\right) = 0.002\ kip$

$F_s := F_{s1} + F_{s2} = 4.196\ lbf$

$$F := F_{pipe} + F_s = 6.032\ lbf$$

Stage 2:

Pipes: $d_1 := \frac{1}{15}\ ft$ $C_{f\_pipe} := 0.7$ $L := \frac{30}{15}\ ft$ $d_2 := \frac{3}{15}\ ft$

$A_{e\_pipe1} := d_1 + 0.1 \cdot \frac{10}{15}\ ft = 0.133\ \frac{ft^2}{ft}$

$F_{pipe1} := q \cdot G \cdot C_{f\_pipe} \cdot A_{e\_pipe1} \cdot L = 0.459\ lbf$

$A_{e\_pipe2} := d_2 + 0.1 \cdot \frac{10}{15}\ ft = 0.267\ \frac{ft^2}{ft}$

$F_{pipe2} := 2 \cdot q \cdot G \cdot C_{f\_pipe} \cdot A_{e\_pipe2} \cdot L = 0.002\ kip$

$F_{pipe} := F_{pipe1} + F_{pipe2} = 0.002\ kip$

Structural members:

First Level: $C_{f\_s} := 2.0$ $h := \frac{12.5}{15}\ ft$

$A_{e\_stringers} := 1 \cdot d \cdot L = 0.163\ ft^2$

$A_{e\_columns} := 4 \cdot b_f \cdot h = 0.272\ ft^2$

$F_{s1} := q \cdot G \cdot C_{f\_s} \cdot \left(A_{e\_stringers} + A_{e\_columns} + 4 \cdot 3.62\ in \cdot 0.25\ in\right) = 0.002\ kip$

Higher Level: $C_{f\_s} := 1.6$ $h := \frac{7.5}{15}\ ft$

$A_{e\_stringers} := 2 \cdot d \cdot L = 0.327\ ft^2$

$A_{e\_columns} := 4 \cdot b_f \cdot h = 0.163\ ft^2$

$F_{s2} := q \cdot G \cdot C_{f\_s} \cdot \left(A_{e\_stringers} + A_{e\_columns}\right) = 0.002\ kip$

$F_s := F_{s1} + F_{s2} = 0.004\ kip$

$F := F_{pipe} + F_s = 6.492\ lbf$

Stage 3:

Pipes: $d_1 := \frac{1}{15}\ ft$ $C_{f\_pipe} := 0.7$ $L := \frac{30}{15}\ ft$ $d_2 := \frac{3}{15}\ ft$

$A_{e\_pipe1} := d_1 + 0.1 \cdot \frac{10}{15}\ ft = 0.133\ \frac{ft^2}{ft}$

$F_{pipe1} := q \cdot G \cdot C_{f\_pipe} \cdot A_{e\_pipe1} \cdot L = \left(4.592 \cdot 10^{-4}\right)\ kip$

$A_{e\_pipe2} := d_2 + 0.1 \cdot \frac{10}{15}\ ft = 0.267\ \frac{ft^2}{ft}$

$F_{pipe2} := q \cdot G \cdot C_{f\_pipe} \cdot A_{e\_pipe2} \cdot L = \left(9.185 \cdot 10^{-4}\right)\ kip$

$A_{e\_pipe3} := d_2 + 0.1 \cdot \frac{20}{15}\ ft = 0.333\ \frac{ft^2}{ft}$

$F_{pipe3} := q \cdot G \cdot C_{f\_pipe} \cdot A_{e\_pipe3} \cdot L = 0.001\ kip$

$F_{pipe} := F_{pipe1} + F_{pipe2} + F_{pipe3} = 0.003\ kip$

Structural members:

First Level: $C_{f\_s} := 2.0$ $h := \frac{12.5}{15}\ ft$

$A_{e\_stringers} := 1 \cdot d \cdot L = 0.163\ ft^2$

$A_{e\_columns} := 4 \cdot b_f \cdot h = 0.272\ ft^2$

$F_{s1} := q \cdot G \cdot C_{f\_s} \cdot \left(A_{e\_stringers} + A_{e\_columns} + 4 \cdot 3.62\ in \cdot 0.25\ in\right) = 0.002\ kip$

Higher Level: $C_{f\_s} := 1.6$ $h := \frac{7.5}{15}\ ft$

$A_{e\_stringers} := 2 \cdot d \cdot L = 0.327\ ft^2$

$A_{e\_columns} := 4 \cdot b_f \cdot h = 0.163\ ft^2$

$F_{s2} := q \cdot G \cdot C_{f\_s} \cdot \left(A_{e\_stringers} + A_{e\_columns}\right) = 0.002\ kip$

$F_s := F_{s1} + F_{s2} = 0.004\ kip$

$$F := F_{pipe} + F_s = 6.721\ lbf$$

Stage 4:

Pipes: $d_1 := \frac{1}{15}\ ft$ $C_{f\_pipe} := 0.7$ $L := \frac{30}{15}\ ft$ $d_2 := \frac{3}{15}\ ft$

$A_{e\_pipe1} := d_1 + 0.1 \cdot \frac{10}{15}\ ft = 0.133\ \frac{ft^2}{ft}$

$F_{pipe1} := q \cdot G \cdot C_{f\_pipe} \cdot A_{e\_pipe1} \cdot L = \left(4.592 \cdot 10^{-4}\right)\ kip$

$A_{e\_pipe2} := d_2 + 0.1 \cdot \frac{20}{15}\ ft = 0.333\ \frac{ft^2}{ft}$

$F_{pipe2} := q \cdot G \cdot C_{f\_pipe} \cdot A_{e\_pipe2} \cdot L = 0.001\ kip$

$A_{e\_pipe3} := d_2 + 0.1 \cdot \frac{20}{15}\ ft = 0.333\ \frac{ft^2}{ft}$

$F_{pipe3} := q \cdot G \cdot C_{f\_pipe} \cdot A_{e\_pipe3} \cdot L = 0.001\ kip$

$F_{pipe} := F_{pipe1} + F_{pipe2} + F_{pipe3} = 0.003\ kip$

Structural members:

First Level: $C_{f\_s} := 2.0$ $h := \frac{12.5}{15}\ ft$

$A_{e\_stringers} := 1 \cdot d \cdot L = 0.163\ ft^2$

$A_{e\_columns} := 4 \cdot b_f \cdot h = 0.272\ ft^2$

$F_{s1} := q \cdot G \cdot C_{f\_s} \cdot \left(A_{e\_stringers} + A_{e\_columns} + 4 \cdot 3.62\ in \cdot 0.25\ in\right) = 0.002\ kip$

Higher Level: $C_{f\_s} := 1.6$ $h := \frac{7.5}{15}\ ft$

$A_{e\_stringers} := 2 \cdot d \cdot L = 0.327\ ft^2$

$A_{e\_columns} := 4 \cdot b_f \cdot h = 0.163\ ft^2$

$F_{s2} := q \cdot G \cdot C_{f\_s} \cdot \left(A_{e\_stringers} + A_{e\_columns}\right) = 0.002\ kip$

$F_s := F_{s1} + F_{s2} = 0.004\ kip$

$$F := F_{pipe} + F_s = 6.951\ lbf$$

Stage 5:

Pipes: $d_1 := \frac{1}{15}\ ft$ $C_{f\_pipe} := 0.7$ $L := \frac{30}{15}\ ft$ $d_2 := \frac{3}{15}\ ft$

$A_{e\_pipe1} := d_1 + 0.1 \cdot \frac{20}{15}\ ft = 0.2\ \frac{ft^2}{ft}$

$F_{pipe1} := q \cdot G \cdot C_{f\_pipe} \cdot A_{e\_pipe1} \cdot L = \left(6.888 \cdot 10^{-4}\right)\ kip$

$A_{e\_pipe2} := d_2 + 0.1 \cdot \frac{20}{15}\ ft = 0.333\ \frac{ft^2}{ft}$

$F_{pipe2} := q \cdot G \cdot C_{f\_pipe} \cdot A_{e\_pipe2} \cdot L = 0.001\ kip$

$A_{e\_pipe3} := d_2 + 0.1 \cdot \frac{20}{15}\ ft = 0.333\ \frac{ft^2}{ft}$

$F_{pipe3} := q \cdot G \cdot C_{f\_pipe} \cdot A_{e\_pipe3} \cdot L = 0.001\ kip$

$F_{pipe} := F_{pipe1} + F_{pipe2} + F_{pipe3} = 0.003\ kip$

Structural members:

First Level: $C_{f\_s} := 2.0$ $h := \frac{12.5}{15}\ ft$

$A_{e\_stringers} := 1 \cdot d \cdot L = 0.163\ ft^2$

$A_{e\_columns} := 4 \cdot b_f \cdot h = 0.272\ ft^2$

$F_{s1} := q \cdot G \cdot C_{f\_s} \cdot \left(A_{e\_stringers} + A_{e\_columns} + 4 \cdot 3.62\ in \cdot 0.25\ in\right) = 0.002\ kip$

Higher Level: $C_{f\_s} := 1.6$ $h := \frac{7.5}{15}\ ft$

$A_{e\_stringers} := 2 \cdot d \cdot L = 0.327\ ft^2$

$A_{e\_columns} := 4 \cdot b_f \cdot h = 0.163\ ft^2$

$F_{s2} := q \cdot G \cdot C_{f\_s} \cdot \left(A_{e\_stringers} + A_{e\_columns}\right) = 0.002\ kip$

$F_s := F_{s1} + F_{s2} = 0.004\ kip$

$F := F_{pipe} + F_s = 7.181\ lbf$
$M := F \cdot 12\ in + F \cdot 8\ in = 143.61\ lbf \cdot in$

SECTION 5.2

Stage 1:

Pipes: $d_{max} := \frac{3}{15}\ ft$ $C_{f\_pipe} := 0.7$ $L := \frac{30}{15}\ ft$

$A_{e\_pipe} := d_{max} + 0.1 \cdot \frac{10}{15}\ ft = 0.267\ \frac{ft^2}{ft}$

$F_{pipe} := 2 \cdot q \cdot G \cdot C_{f\_pipe} \cdot A_{e\_pipe} \cdot L = 1.837\ lbf$

Structural members:

$b_f = 0.98\ in$ $d = 0.98\ in$ $h := \frac{20}{15}\ ft$

$A_s := (4 \cdot h \cdot d) + (9 \cdot d \cdot (8\ in - d)) + 4 \cdot 3.62\ in \cdot 0.25\ in = 128.256\ in^2$

$A_g := h \cdot (L + d) = 399.68\ in^2$

$\varepsilon := \frac{A_s}{A_g} = 0.321$

$N := 2$ $S_f := \frac{10}{15}\ ft$ $B := L + d = 24.98\ in$ $\frac{S_f}{B} = 0.32$

$C_{Dg} := 0.72$ Figure 5.1

$C_f := \frac{C_{Dg}}{\varepsilon} = 2.244$

$F_s := q \cdot G \cdot C_f \cdot A_s = 4.916\ lbf$

$F := F_s + F_{pipe} = 6.753\ lbf$

Stage 2:

Pipes: $d_1 := \frac{1}{15}\ ft$ $C_{f\_pipe} := 0.7$ $L := \frac{30}{15}\ ft$ $d_2 := \frac{3}{15}\ ft$

$A_{e\_pipe1} := d_1 + 0.1 \cdot \frac{10}{15}\ ft = 0.133\ \frac{ft^2}{ft}$

$F_{pipe1} := q \cdot G \cdot C_{f\_pipe} \cdot A_{e\_pipe1} \cdot L = 0.459\ lbf$

$A_{e\_pipe2} := d_2 + 0.1 \cdot \frac{10}{15}\ ft = 0.267\ \frac{ft^2}{ft}$

$F_{pipe2} := 2 \cdot q \cdot G \cdot C_{f\_pipe} \cdot A_{e\_pipe2} \cdot L = 1.837\ lbf$

$F_{pipe} := F_{pipe1} + F_{pipe2} = 2.296\ lbf$

Structural members:

$b_f = 0.98\ in$ $d = 0.98\ in$ $h := \frac{20}{15}\ ft$

$A_s := (4 \cdot h \cdot d) + (9 \cdot d \cdot (8\ in - d)) + 4 \cdot 3.62\ in \cdot 0.25\ in = 128.256\ in^2$

$A_g := h \cdot (L + d) = 399.68\ in^2$

$\varepsilon := \frac{A_s}{A_g} = 0.321$

$N := 2$ $S_f := \frac{10}{15}\ ft$ $B := L + d = 24.98\ in$ $\frac{S_f}{B} = 0.32$

$C_{Dg} := 0.72$ Figure 5.1

$C_f := \frac{C_{Dg}}{\varepsilon} = 2.244$

$F_s := q \cdot G \cdot C_f \cdot A_s = 4.916\ lbf$

$F := F_{pipe} + F_s = 7.213\ lbf$

Stage 3:

Pipes: $d_1 := \frac{1}{15}\ ft$ $C_{f\_pipe} := 0.7$ $L := \frac{30}{15}\ ft$ $d_2 := \frac{3}{15}\ ft$

$A_{e\_pipe1} := d_1 + 0.1 \cdot \frac{10}{15}\ ft = 0.133\ \frac{ft^2}{ft}$

$F_{pipe1} := q \cdot G \cdot C_{f\_pipe} \cdot A_{e\_pipe1} \cdot L = \left(4.592 \cdot 10^{-4}\right)\ kip$

$A_{e\_pipe2} := d_2 + 0.1 \cdot \frac{10}{15}\ ft = 0.267\ \frac{ft^2}{ft}$

$F_{pipe2} := q \cdot G \cdot C_{f\_pipe} \cdot A_{e\_pipe2} \cdot L = \left(9.185 \cdot 10^{-4}\right)\ kip$

$A_{e\_pipe3} := d_2 + 0.1 \cdot \frac{20}{15}\ ft = 0.333\ \frac{ft^2}{ft}$

$F_{pipe3} := q \cdot G \cdot C_{f\_pipe} \cdot A_{e\_pipe3} \cdot L = 0.001\ kip$

$F_{pipe} := F_{pipe1} + F_{pipe2} + F_{pipe3} = 0.003\ kip$

Structural members:

$b_f = 0.98\ in$ $d = 0.98\ in$ $h := \frac{20}{15}\ ft$

$A_s := (4 \cdot h \cdot d) + (9 \cdot d \cdot (8\ in - d)) + 4 \cdot 3.62\ in \cdot 0.25\ in = 128.256\ in^2$

$A_g := h \cdot (L + d) = 399.68\ in^2$

$\varepsilon := \frac{A_s}{A_g} = 0.321$

$N := 2$ $S_f := \frac{10}{15}\ ft$ $B := L + d = 24.98\ in$ $\frac{S_f}{B} = 0.32$

$C_{Dg} := 0.72$ Figure 5.1

$C_f := \frac{C_{Dg}}{\varepsilon} = 2.244$

$F_s := q \cdot G \cdot C_f \cdot A_s = 4.916\ lbf$

$F := F_{pipe} + F_s = 7.442\ lbf$

Stage 4:

Pipes: $d_1 := \frac{1}{15}\ ft$ $C_{f\_pipe} := 0.7$ $L := \frac{30}{15}\ ft$ $d_2 := \frac{3}{15}\ ft$

$A_{e\_pipe1} := d_1 + 0.1 \cdot \frac{10}{15}\ ft = 0.133\ \frac{ft^2}{ft}$

$F_{pipe1} := q \cdot G \cdot C_{f\_pipe} \cdot A_{e\_pipe1} \cdot L = \left(4.592 \cdot 10^{-4}\right)\ kip$

$A_{e\_pipe2} := d_2 + 0.1 \cdot \frac{20}{15}\ ft = 0.333\ \frac{ft^2}{ft}$

$F_{pipe2} := q \cdot G \cdot C_{f\_pipe} \cdot A_{e\_pipe2} \cdot L = 0.001\ kip$

$A_{e\_pipe3} := d_2 + 0.1 \cdot \frac{20}{15}\ ft = 0.333\ \frac{ft^2}{ft}$

$F_{pipe3} := q \cdot G \cdot C_{f\_pipe} \cdot A_{e\_pipe3} \cdot L = 0.001\ kip$

$F_{pipe} := F_{pipe1} + F_{pipe2} + F_{pipe3} = 0.003\ kip$

Structural members:

$b_f = 0.98\ in$ $d = 0.98\ in$ $h := \frac{20}{15}\ ft$

$A_s := (4 \cdot h \cdot d) + (9 \cdot d \cdot (8\ in - d)) + 4 \cdot 3.62\ in \cdot 0.25\ in = 128.256\ in^2$

$A_g := h \cdot (L + d) = 399.68\ in^2$

$\varepsilon := \frac{A_s}{A_g} = 0.321$

$N := 2$ $S_f := \frac{10}{15}\ ft$ $B := L + d = 24.98\ in$ $\frac{S_f}{B} = 0.32$

$C_{Dg} := 0.72$ Figure 5.1

$C_f := \frac{C_{Dg}}{\varepsilon} = 2.244$

$F_s := q \cdot G \cdot C_f \cdot A_s = 4.916\ lbf$

$F := F_s + F_{pipe} = 7.672\ lbf$

Stage 5:

Pipes: $d_1 := \frac{1}{15}\ ft$ $C_{f\_pipe} := 0.7$ $L := \frac{30}{15}\ ft$ $d_2 := \frac{3}{15}\ ft$

$A_{e\_pipe1} := d_1 + 0.1 \cdot \frac{20}{15}\ ft = 0.2\ \frac{ft^2}{ft}$

$F_{pipe1} := q \cdot G \cdot C_{f\_pipe} \cdot A_{e\_pipe1} \cdot L = \left(6.888 \cdot 10^{-4}\right)\ kip$

$A_{e\_pipe2} := d_2 + 0.1 \cdot \frac{20}{15}\ ft = 0.333\ \frac{ft^2}{ft}$

$F_{pipe2} := q \cdot G \cdot C_{f\_pipe} \cdot A_{e\_pipe2} \cdot L = 0.001\ kip$

$A_{e\_pipe3} := d_2 + 0.1 \cdot \frac{20}{15}\ ft = 0.333\ \frac{ft^2}{ft}$

$F_{pipe3} := q \cdot G \cdot C_{f\_pipe} \cdot A_{e\_pipe3} \cdot L = 0.001\ kip$

$F_{pipe} := F_{pipe1} + F_{pipe2} + F_{pipe3} = 0.003\ kip$

Structural members:

$b_f = 0.98\ in$ $d = 0.98\ in$ $h := \frac{20}{15}\ ft$

$A_s := (4 \cdot h \cdot d) + (9 \cdot d \cdot (8\ in - d)) + 4 \cdot 3.62\ in \cdot 0.25\ in = 128.256\ in^2$

$A_g := h \cdot (L + d) = 399.68\ in^2$

$\varepsilon := \frac{A_s}{A_g} = 0.321$

$N := 2$ $S_f := \frac{10}{15}\ ft$ $B := L + d = 24.98\ in$ $\frac{S_f}{B} = 0.32$

$C_{Dg} := 0.72$ Figure 5.1

$C_f := \frac{C_{Dg}}{\varepsilon} = 2.244$

$F_s := q \cdot G \cdot C_f \cdot A_s = 4.916\ lbf$

$F := F_{pipe} + F_s = 7.901\ lbf$

$M := F \cdot 12\ in + F \cdot 8\ in = 158.028\ lbf \cdot in$